nature communications

Article

https://doi.org/10.1038/s41467-024-52076-0

Molecular mechanism of IKK catalytic dimer docking to NF-κB substrates

Received: 27 August 2023

Accepted: 27 August 2024

Published online: 03 September 2024

Check for updates

Changqing Li[1,8], Stefano Moro[1,8], Kateryna Shostak[2], Francis J. O'Reilly[3], Mariel Donzeau[1], Andrea Graziadei[3], Alastair G. McEwen[4], Dominique Desplancq[1], Pierre Poussin-Courmontagne[4], Thomas Bachelart[1], Mert Fiskin[1], Nicolas Berrodier[4], Simon Pichard[4], Karl Brillet[5], Georges Orfanoudakis[1], Arnaud Poterszman[4], Vladimir Torbeev[1], Juri Rappsilber[3], Norman E. Davey[6], Alain Chariot[2,7] & Katia Zanier[1]

The inhibitor of κB (IκB) kinase (IKK) is a central regulator of NF-κB signaling. All IKK complexes contain hetero- or homodimers of the catalytic IKKβ and/or IKKα subunits. Here, we identify a YDDΦxΦ motif, which is conserved in substrates of canonical (IκBα, IκBβ) and alternative (p100) NF-κB pathways, and which mediates docking to catalytic IKK dimers. We demonstrate a quantitative correlation between docking affinity and IKK activity related to IκBα phosphorylation/degradation. Furthermore, we show that phosphorylation of the motif's conserved tyrosine, an event previously reported to promote IκBα accumulation and inhibition of NF-κB gene expression, suppresses the docking interaction. Results from integrated structural analyzes indicate that the motif binds to a groove at the IKK dimer interface. Consistently, suppression of IKK dimerization also abolishes IκBα substrate binding. Finally, we show that an optimized bivalent motif peptide inhibits NF-κB signaling. This work unveils a function for IKKα/β dimerization in substrate motif recognition.

Nuclear factor κB (NF-κB) signaling plays a central role in the regulation of cellular inflammatory, immune, and apoptotic responses[1]. Under homeostatic conditions, NF-κB dimers are sequestered in the cytoplasm by interaction with inhibitor of κB (IκB) proteins or with the NF-κB precursor proteins p100 and p105. Receptor stimulation of the 'canonical' NF-κB pathway activates the inhibitor of κB (IκB) kinase (IKK), which, in turn, phosphorylates IκB proteins. This results in the ubiquitin-mediated degradation of IκB and subsequent nuclear translocation of p65/p50 NF-κB dimers[2]. Stimulation of the 'alternative' NF-κB pathway leads instead to IKK-mediated phosphorylation of p100, which triggers partial degradation of p100 into the mature p52 NF-κB subunit[2].

Different IKK complexes (collectively referred to as IKKs hereafter) exist in cells and exhibit variable subunit composition. The core of the canonical IKK complex comprises a heterodimer of the catalytic IKKα/1 and IKKβ/2 subunits (named IKKα and IKKβ hereafter) and two copies of the regulatory NEMO subunit[3–5]. Whereas IKKα contributes to kinase activation by phosphorylating the IKKβ activation loop[6], the IKKβ subunit directly phosphorylates a phospho-dependent D_pSGxx_pS/T βTrCP degron motif (where pS or pT are phosphoserine

[1]Biotechnology and Cell Signaling (CNRS/Université de Strasbourg, UMR7242), Ecole Superieure de Biotechnologie de Strasbourg, Boulevard Sébastien Brant, 67400 Illkirch, France. [2]Laboratory of Cancer Biology, GIGA Cancer, University of Liege, CHU, Sart-Tilman, 4000 Liege, Belgium. [3]Institute of Biotechnology, Technische Universität Berlin, Gustav-Meyer-Allee 25, Berlin, Germany. [4]Institut de Génétique et de Biologie Moléculaire et Cellulaire (IGBMC) / INSERM UMR-S 1258 / CNRS UMR7104/ Université de Strasbourg, 1 rue Laurent Fries, 67400 Illkirch, France. [5]Institut Biologie Moléculaire et Cellulaire (IBMC), CNRS UPR9002, 2 allée Konrad Roentgen, 67000 Strasbourg, France. [6]Division of Cancer Biology, The Institute of Cancer Research, 237 Fulham Road, London SW3 6JB, UK. [7]WELBIO department, WEL Research Institute, avenue Pasteur, 6, 1300 Wavre, Belgium. [8]These authors contributed equally: Changqing Li, Stefano Moro. e-mail: zanier@unistra.fr

or phosphothreonine and x is any amino acid) of IκB proteins[7]. Upon phosphorylation, this motif is bound by the βTrCP-containing subunit of the SCF E3 ligase complex, leading to polyubiquitination and degradation of IκB proteins[8]. In contrast, the core of the complex acting in the alternative pathway consists of a homodimer of IKKα[9,10].

Seminal work on the IKKα and IKKβ homodimers has revealed striking structural similarities, which are linked to the high sequence homology between these two subunits[11–14]. Both subunits share an identical architecture, which comprises an N-terminal kinase domain (KD), a ubiquitin-like domain (ULD), a helical scaffold dimerization domain (SDD), and a C-terminal NEMO binding domain. Dimerization is essentially mediated by the C-terminal portion of the SDD domain. For both IKKα and IKKβ, multiple dimer conformations have been observed, which differ in the extent of splaying apart of the KD-ULD portions. Such conformations are thought to be related to kinase activity. In particular, it has been proposed that an 'open' state of the dimer permits higher order oligomerization, which, in turn, contributes to kinase activation through a *trans*-autophosphorylation mechanism[12,13].

NEMO is an obligate scaffolding protein[15], consisting of an N-terminal region exhibiting high affinity for IKKβ, an extensive central coil-coil interspersed by disordered segments, and a C-terminal zinc-finger domain[16,17]. NEMO mediates activation of the canonical IKK complex by binding to polyubiquitin chains (polyUb) via its NOA/UBAN motif and the C-terminal zinc finger[18–20]. Recent studies have shown that multivalent NEMO/polyUb interactions drive the in vivo formation of lattice structures of IKK displaying liquid-like droplet properties, which are associated with IKK activation[21,22].

The canonical complex is the most abundant IKK species in cells in stimulated conditions. However, IKKα and IKKβ also act as part of different IKKs on a variety of substrates involved in key cellular functions[23]. In particular, IKKα homodimers play important roles in the nucleus by phosphorylating transcription factors such as IRF7[24], co-activators, and co-repressors, including SMRT, CBP, SRC-3 ([25] and references therein), and histone H3[26,27]. IKKβ has instead been shown to act on several tumor suppressor pathways, including FOXO3a, TSC1, and p53 ([25] and references therein).

Many kinases achieve high specificity by docking interactions that involve the recognition of Short Linear Motifs (SLiMs), which are distinct from the substrate motif recognized by the active site of the enzyme[28]. The NEMO subunit has been reported to interact with the IκBα substrate protein via its C-terminal zinc-finger domain[15]. However, since NEMO is not present in the alternative IKK complex, additional mechanisms must exist to mediate substrate recruitment to the kinase. In this work, we describe the identification and characterization of a SLiM that mediates docking of IKKα/β dimers to partner proteins in NF-κB signaling.

Results

IKKα and IKKβ dock to a YDDΦxΦ motif within IκBα

IκBα, the canonical substrate of IKK, comprises a disordered N-terminal region, which contains phospho-Ser32 and phospho-Ser36 residues that are part of the D_pSGxx_pS/T βTrCP degron motif, an ankyrin repeat domain (ARD) and a disordered C-terminal region containing a PEST sequence (Fig. 1a). To identify the IκBα region interacting with the IKKβ subunit, we performed in vitro pulldown experiments employing recombinant purified proteins. We produced IκBα constructs fused to the C-terminus of the maltose binding protein (MBP) and a nearly full-length (residues 1-669) and constitutively active (S177E/S181E) mutant construct of human IKKβ (named IKKβ (1-669) EE hereafter), which resembles the previously crystallized fragment of this protein[12,14]. The IKKβ homodimer was purified by affinity and size exclusion chromatography (see Methods section).

The interaction of the IKKβ homodimer with full-length IκBα becomes clearly visible at relatively high concentrations of IKKβ (Fig. 1b, compare *left panel* - 5 μM of IKKβ - with *right panel* - 0.4 μM of IKKβ). Unexpectedly, deletion of the N-terminal region of IκBα enhances binding to IKKβ (Fig. 1b *right panel*, compare FL IκBα with IκBα(73-317), which is named IκBαΔ73 hereafter). In contrast, further deletion of the C-terminal region abolishes the interaction (Fig. 1b *right panel*, compare IκBαΔ73 with IκBα(73-288), which is named IκBαΔ73ΔC hereafter). Subsequent dissection of the C-terminus of IκBα identified a 17 amino acid peptide (residues 301-317 of IκBα, named IκBα pep(s) hereafter), which is necessary and sufficient for interaction with IKKβ at levels comparable to the N-terminal truncated construct (Fig. 1b *right panel*, compare IκBαΔ73 with IκBα pep(s)). Serine mutagenesis of IκBα pep(s) indicates that Tyr305, Asp306, Asp307, Cys308 and Phe310 residues are essential for the interaction with IKKβ (Supplementary Fig. 1a). Consistently, sequence alignments (Fig. 1c) reveal that these residues are conserved in IκBα proteins from different species and are part of a motif with a $Y_1D_2D_3\Phi_4x_5\Phi_6$ consensus (where Y is a tyrosine, D is an aspartic acid, Φ is a hydrophobic amino acid and x is any amino acid). This motif is flanked on the N-terminal side by a patch of acidic residues (residues 297-302) that are conserved across species.

Next, we analyzed IKK interactions with IκBα *in cellulo* using the *Gaussia princeps* protein complementation assay (GPCA)[4]. Here, full-length IKKα or IKKβ proteins and IκBα constructs were fused to the C-terminal extremities of the G1 and G2 fragments of the *Gaussia* luciferase, respectively. Pairwise combinations of G1-IKKα or G1-IKKβ and G2-IκBα were then co-transfected in HEK293T cells and the interactions monitored following the activity of the reconstituted luciferase. We found that both IKKα and IKKβ interact with full-length IκBα, with IKKα showing higher binding responses (Fig. 1d). In line with the pulldown results, truncation of the N-terminal region of IκBα again enhances binding to both IKKα and IKKβ (Fig. 1d, compare IκBα FL with IκBαΔ73). A possible explanation for this finding might be a steric hindrance effect of the N-terminal region of IκBα occurring when the p50/p65 NF-κB dimer is not bound to the ARD domain, a mechanism which may be related to the previously observed ability of IKK to discriminate between free and NF-κB bound IκBα substrate[29]. In contrast, further deletion of the disordered C-terminal region or the double serine substitution at positions Y_1 and D_3 of the motif (i.e. Y305S/D307S, named YD/SS hereafter) strongly decreases the interactions to both IKK homodimers (Fig. 1d, compared IκBαΔ73 with IκBαΔ73ΔC and IκBαΔ73 YD/SS).

We then proceeded to reconstitute the IKKα/β heterodimer by co-expression of 6xHis-IKKβ(1-669) EE and Strep-IKKα(10-667) EE constructs in insect cells and purification by two consecutive affinity-chromatography steps (Ni^{2+}-NTA and Strep-Tactin) plus gel filtration (see Methods section). The results from MBP-pulldown analyzes show that the IKKα/β heterodimer specifically binds to IκBα pep(s) (Fig. 1e).

To evaluate binding affinities, we performed isothermal titration calorimetry (ITC) experiments using a synthetic peptide that comprises the YDDΦxΦ motif plus the N-terminal acidic patch (residues 297-317, named IκBα pep hereafter, Fig. 2a) and purified IKKβ(1-669) EE homodimer or an equivalent construct of the IKKα homodimer (i.e. IKKα(10-667) S176E/S180E[13], named IKKα(10-667) EE hereafter). The results indicate significantly higher affinity for the interaction with IKKα (K_D = 7.7 μM) as compared to IKKβ (K_D = 40 μM) (Table 1 and Fig. 2b, c). In contrast, ITC analyzes on the IKKα/β heterodimer were prevented by strong sample aggregation at the concentrations required for these experiments.

In the next step, we introduced single amino acid substitutions at the conserved positions of the motif of IκBα pep(s) (i.e. Y_1, D_2, D_3, Φ_4 and Φ_6) and evaluated the impact on the interactions with purified IKK homodimers. Most of the mutations have a negative effect on the interactions with IKKβ, whereas IKKα appears to tolerate a higher number of substitutions, particularly at positions Y_1, D_2 and Φ_6 (Fig. 1f and Supplementary Fig. 1b, c). In contrast, two substitutions at the Φ_4

https://doi.org/10.1038/s41467-024-52076-0

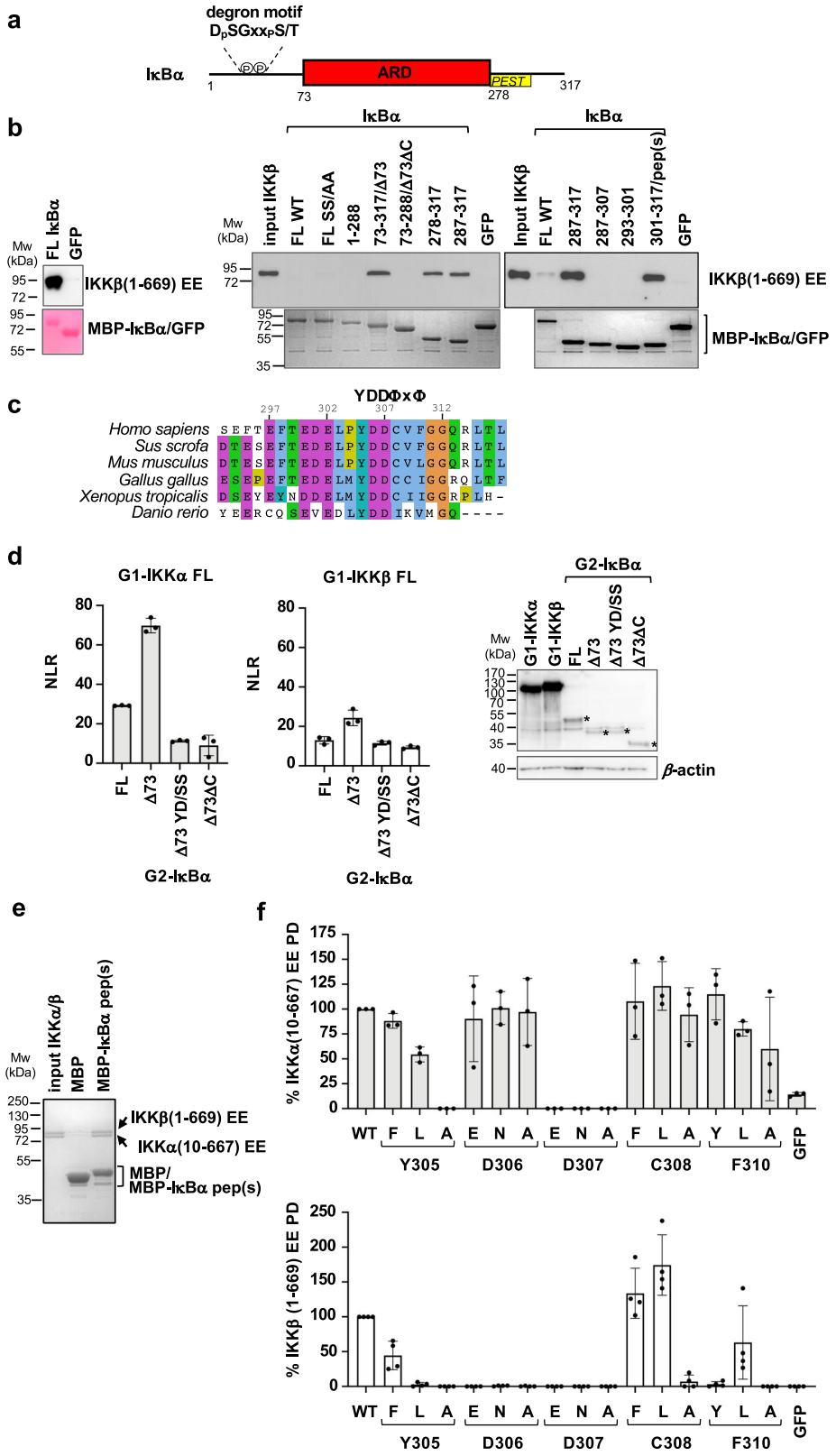

position, i.e. C308L and C308F, appear to enhance binding to IKKβ (Fig. 1f *lower panel*). Consistently, ITC analyzes show that the C308L substitution increases IκBα pep affinities to both IKKα and IKKβ, by aproximately 20- and 15-fold, respectively (K_D = 420 nM for IKKα and K_D = 2.4 μM for IKKβ) (Table 1 and Fig. 2b, c).

Together, these results demonstrate that homo- and heterodimers of the catalytic IKKα and IKKβ subunits dock to a YDDΦxΦ motif located in the C-terminal region of the IκBα substrate. This is in agreement with binding data from Xu and coworkers[11], who suggested the existence of an exosite for IKKβ within the C-terminal region of IκBα[11]. Based on our findings, the motif seems to have significantly higher affinity for IKKα compared to IKKβ. Finally, amino acid replacements within the motif's consensus enable us to modulate the affinity of the interaction in both positive and negative ways.

Fig. 1 | IKKα and IKKβ interactions with the YDDΦxΦ motif of IκBα. a Domain architecture of IκBα. N-terminal region containing substrate degron motif (residues 1-72); ARD: ankyrin repeat domain (residues 73-278); C-ter region containing the PEST sequence (residues 278-317). **b** Pulldown analyzes using 6xHis-IKKβ(1-669) EE and MBP-IκBα constructs coupled to amylose resin. The IKKβ concentrations were adjusted to 5 µM (*left panel*) or to 0.4 µM (*right panel*). MBP-GFP: negative control. (*Left panel*) Samples were migrated on two separate 10% SDS-PAGE gels, to detect IKKβ by Western blot (anti-His antibody) and MBP-IκBα by Coomassie staining, respectively. IκBα constructs 73–317, 73–288, and 301–317 are named Δ73, Δ73ΔC and pep(s), respectively. These interactions were reproduced in a second independent pulldown experiment. **c** Sequence alignment of residues 293-317 of human IκBα highlighting the YDDΦxΦ consensus. **d** (*Left and middle panels*) Representative GPCA datasets for the interactions of full-length wt IKKα and IKKβ proteins with IκBα constructs in HEK293T cells. IKK and IκBα constructs were fused to the G1 and G2 fragments of the luciferase, respectively. YD/SS: Y305S/D307S mutation in IκBα. NLR: normalized luminescence ratio (see methods section). The data (mean +/− SD) are derived from three independent transfection experiments. (*Right panel*) Western blot analysis of the expression levels of G1-IKKα, G1-IKKβ, and G2-IκBα (indicated by asterisks) constructs in HEK293T cells using an anti-luciferase antibody. **e** Pulldowns using purified IKKα/β heterodimer (reconstituted from 6xHis-IKKβ(1-669) EE and Strep-IKKα(10-667) EE constructs) and MBP-IκBα pep(s) or MBP negative control. IKK and MBP-fusion proteins were visualized by Coomassie stain. **f** Results from pulldown analyzes of the interactions of 6xHis-IKKα(10-667) EE (*upper panel*) or 6xHis-IKKβ(1-669) EE (*lower panel*) with MBP-IκBα pep(s) mutants. Three single amino acid substitutions were tested for each conserved position of the YDDΦxΦ consensus. IKKα or IKKβ bands were quantified and the data normalized to the interactions of IκBα pep(s) wt to IKKα or IKKβ (100%). For each panel, all interactions were processed in parallel (see Source Data file). The data (mean +/− SD) are derived from three ($n = 3$, *upper panel*) or four ($n = 4$, *lower panel*) independent pulldown experiments. See also Supplementary Fig. 1b, c for gel images. Source data for this figure are provided as a Source Data file.

Docking affinity correlates with IKK activity

We assessed the impact of the docking interaction on IKK activity. To mimic in vivo conditions as previously described[15], we performed in vitro kinase experiments in the presence of high concentrations of a nonspecific competitor protein (BSA), limiting concentrations of purified full-length wt or mutant IκBα proteins and endogenous canonical IKK that was immunoprecipitated from HEK293T cells using an anti-NEMO antibody. The results show that Ser32/Ser36 phosphorylation is highest for the IκBα C308L mutant with improved docking affinity, whereas IκBα YD/SS is not phosphorylated under these assay conditions (Fig. 3a). Similar results were obtained using recombinant purified IKKβ(1-669) EE instead of the endogenous canonical complex (Supplementary Fig. 2a).

We also evaluated the degradation profiles of wt or mutant IκBα proteins upon activation of the canonical NF-κB pathway. In these experiments, IκBα constructs are retro-transduced in mouse embryonic fibroblast (MEF) lacking IκB family genes (MEF IκBα/IκBβ/IκBε KO) and their protein levels monitored at selected time points after TNFα stimulation. As expected, the S32A/S36A (SS/AA) mutation targeting phospho-acceptor residues completely suppresses IκBα degradation, as evidenced by the lack of change in IκBα levels following TNFα stimulation (Fig. 3b). Mutations at the YDDΦxΦ docking motif have milder effects on IκBα levels. The degradation of the IκBα YD/SS mutant appears to be slower, whereas the degradation of the higher affinity IκBα C308F mutant, which is used here due to the low expression levels of IκBα C308L in MEFs (Supplementary Fig. 2b), is slightly faster compared to that of the wt IκBα protein (Fig. 3b).

Taken together, these results show that the affinity of the docking interaction correlates with both phosphorylation and degradation of the IκBα substrate. Yet, the residual degradation activity of the IκBα YD/SS mutant observed here indicates that additional determinants contribute to substrate recruitment, which may involve the NEMO interaction with IκBα[15].

Docking is negatively regulated by a phosphorylation switch

The Y_1 (Tyr305) position of the docking motif is a strictly conserved tyrosine (Fig. 1c), which suggests that it may be a target of phosphorylation. To explore this possibility, HA-IκBα and HA-IκBαΔ73 proteins transiently expressed in HEK293T cells were immunoprecipitated and analyzed by Western blot using an anti-phospho-Tyr antibody. Results show that tyrosine phosphorylation of IκBα becomes detectable only when cells are treated with the protein tyrosine phosphatase (PTP) inhibitor pervanadate (Fig. 3c *top and middle panels*, compare pY-IκBα and pY-IκBαΔ73 bands). Remarkably, the conservative Y305F mutation reduces phosphorylation in full-length IκBα, while it completely suppresses it in the IκBαΔ73 construct, indicating that Tyr305 is the only phosphorylated tyrosine between residues 73 and 317 of IκBα under steady-state conditions (Fig. 3c top *panel*, lanes 6–7, and 8–9). On the other hand, TNFα stimulation does not appear to induce degradation of full-length IκBα, indicating that the pervanadate treatment impairs activation of the canonical pathway (Fig. 3c, lanes 10-13 of *top and bottom panels* and Supplementary Fig. 2c), and thereby preventing us from evaluating the phosphorylation state of Tyr305 during NF-κB signaling.

We thus investigated the impact of Y_1 phosphorylation on docking by ITC, by titrating the IKKα homodimer, which displays higher affinity for the YDDΦxΦ motif as compared to IKKβ, with a synthetic phospho-Tyr305 IκBα pep (named pY-IκBα pep hereafter) peptide. The enthalpy (ΔH) term obtained is zero, which suggests an absence of interaction (Fig. 3d). To rule out the possibility that the zero ΔH value is accidental (i.e. arising as a consequence of the van't Hoff rule), we performed MBP-pulldown experiments in the presence of increasing concentrations of competitor synthetic peptides. Whereas IκBα pep competes with MBP-IκBα pep for binding to IKKα, phosphorylated pY-IκBα pep does not appear to affect the IKKα/MBP-IκBα pep interaction (Fig. 3e).

To conclude, we demonstrate that phosphorylation at Y_1 (Tyr305) drastically diminishes the binding affinity for IKK dimers. This position is phosphorylated under steady-state conditions. Interestingly, an independent study reported that Tyr305 phosphorylation is enhanced upon genotoxic stress and that this leads to IκBα accumulation and, consequently, inhibition of NF-κB gene expression[30]. Together, these findings suggest that a phosphorylation switch at Y_1 may serve as a safeguard mechanism to prevent unwanted substrate phosphorylation of the N-terminal βTrCP degron motif of IκBα.

YDDΦxΦ motif-containing peptides inhibit NF-κB signaling

The MBP-IκBα pep fusion comprising the C308L mutation is able to capture endogenous IKKβ from clarified extracts of HEK293T cells (Supplementary Fig. 3a). This raises the possibility that docking motif peptides could act as competitive inhibitors of IKK-substrate interactions. Consistently, results from in vitro kinase experiments performed in the presence of synthetic IκBα pep variants indicate that both wt and C308L peptides inhibit IκBα phosphorylation more efficiently than the YD/SS negative control peptide (Fig. 4a).

To improve binding activity for in vivo studies, we created bivalent peptides by fusing the IκBα pep sequence to the E3 tag, a peptide derived from the oligomerization domain of p53, which was engineered to mediate the formation of strong homodimers[31]. The E3-IκBα pep constructs were appended to the C-terminus of the mScarlet protein for fluorescent detection (Fig. 4b). These mScarlet-E3-IκBα pep fusions were then transfected as mRNAs into human fetal lung fibroblast (MRC-5) and activation of canonical NF-κB signaling was monitored by following nuclear translocation of p65. As expected, in unstimulated conditions p65 is found in the cytoplasm (Fig. 4c *left panel*). Upon TNFα induction, p65 translocates into the nucleus only in the case of the fusion containing the IκBα pep YD/SS

https://doi.org/10.1038/s41467-024-52076-0

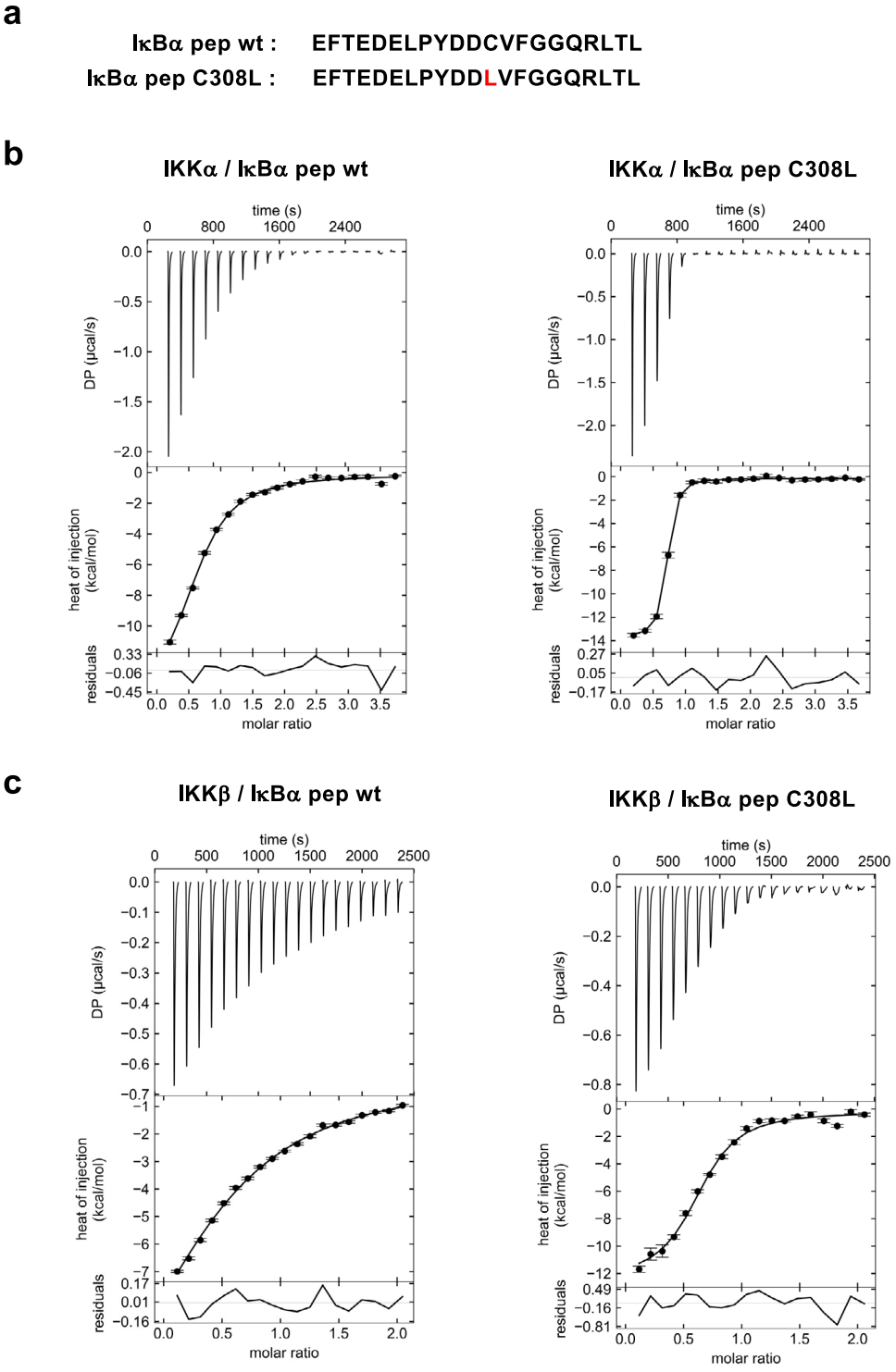

Fig. 2 | ITC analysis of the IKKα and IKKβ interactions with IκBα pep. **a** Sequences of the IκBα pep wt and C308L synthetic peptides. **b**, **c** Representative ITC binding isotherms for the indicated interactions. The experiments used purified IKKα(10-667) EE or IKKβ(1-669) EE proteins at concentrations between 22 and 50 µM, depending on the experiment, and peptide concentrations were adjusted accordingly (i.e. between 220 and 975 µM). DP: differential power. The data were analyzed by global fitting (see Table 1). The residuals are calculated as differences between fitted and experimental values, whereas the error bars correspond to the root-mean-square-deviation (RMSD) of the fitted and measured injection data as implemented in SEDPHAT[61]. Each interaction was measured in at least two independent ITC titration experiments. Source data are provided as a Source Data file.

negative control sequence, whereas the IκBα pep C308L sequence efficiently retains p65 in the cytoplasm at levels comparable to the unstimulated condition (Fig. 4c *left and right panels* and Supplementary Fig. 3b).

These results provide evidence that the docking mechanism is active during signaling and that it can be blocked by YDDΦxΦ peptides leading to inhibition of the canonical NF-κB pathway.

Table 1 | Thermodynamic parameters of IKKα or IKKβ binding to YDDΦXΦ peptides

interaction	*N*	*K_D (μM)*	*ΔH (kcal/mol)*	*TΔS (kcal/mol)*	*ΔG (kcal/mol)*
IKKα / IκBα pep wt	0.63	7.7 (6.5, 9.4)	−14.2 (−15.5, −13.2)	−7.23	−6.97
IKKα / IκBα pep C308L	0.65	0.42 (0.33, 0.55)	−13.7 (−14.1, −13.4)	−5.01	−8.69
IKKα / pY-IκBα pep	*N.D.*	*N.D.*	*N.D.*	*N.D.*	*N.D.*
IKKβ / IκBα pep wt	0.63	40 (35, 46)	−16.3 (−19.3, −14.2)	−10.3	−6.00
IKKβ / IκBα pep C308L	0.66	2.4 (1.7, 3.1)	−11.5 (−12.1, −10.8)	−3.83	−7.67
IKKα / p100 pep	0.60*	12** (3.5, 18)	−13.4** (−17.2, −8.30)	−6.69	−6.71
IKKα / IRF7 pep	*N.D.*	*N.D.*	*N.D.*	*N.D.*	*N.D.*

All ITC experiments were performed at 25 °C. The data were fitted to a 1:1 binding model. *N* refers to the binding stoichiometry of IKKα/β: pep. Data were processed using the NITPIC software[60]. For each interaction, the thermodynamic parameters were derived from the global fitting of two independent titration curves ($n = 2$) using the SEDPHAT software[61]. For the best-fit values of K_D and ΔH, a confidence interval at 68.3% probability (one SD assuming a Gaussian error distribution) was calculated (in brackets) using error surfaces prescribed by F-statistics.
*value constrained during fitting.
**broad confidence intervals correspond to poor convergence, therefore, for this titration fitted values should be considered as estimates.
N.D. not determined.

Structural studies of the IKKβ/IκBα pep complex

We carried out several crystallization screenings on samples of IKKα or IKKβ homodimers bound to synthetic IκBα pep wt or C308L peptides. Most crystals obtained displayed poor x-ray diffraction patterns, reflecting previously reported difficulties linked to high-resolution structural studies on these dimers[13]. Nevertheless, we were able to identify one crystal grown from a sample of IKKβ(1-669) EE mixed with wt IκBα pep, which diffracted synchrotron radiation to a resolution of 4.15-6.8 Å (anisotropic diffraction, see Supplementary Table 1), allowing for structure determination by molecular replacement. The asymmetric unit of the crystal contains five IKKβ protomers. Four protomers form two distinct homodimers (A-B and C-D) with the characteristic "scissor-like" structure mediated by contacts involving the C-terminal portions of the SDD domains (Fig. 5a and Supplementary Fig. 4a). The fifth protomer of the unit cell homodimerizes with its symmetry equivalent molecule from a neighboring asymmetric unit. The conformations of the A-B and C-D homodimers differ in the extent of the splaying apart of the KD-ULD portions, with the A-B homodimer displaying a relatively 'closed' conformation compared to the C-D homodimer (Supplementary Fig. 4b, c). B-factor analysis indicates lower flexibility for the helices of the SDD domain in the A-B homodimer than in the C-D homodimer (Supplementary Fig. 4d).

Whereas our data recapitulate previously observed structural features of IKKβ, we were unable to clearly observe electron density for the IκBα pep ligand due to the lack of high resolution. We therefore turned to cross-linking mass spectrometry (CLMS)[32] to independently map the binding site of IκBα pep on IKKβ. For this, purified IKKβ(1-669) EE was mixed with a 10-fold molar excess of synthetic IκBα pep C308L/R314K, which incorporates an additional Arg to Lys substitution to improve peptide cross-linking efficiency. Protein samples were cross-linked using three distinct agents with different chemistries and spacer lengths: EDC/sulfo-NHS, sulfo-SDA and BS3. Protein-peptide cross-linked species were isolated by migration on SDS-PAGE (Supplementary Fig. 5a–c) and analyzed by MS.

Despite the large excess of peptide added, the totality of the intermolecular IKKβ-peptide cross-links identified in the different samples map to the SDD domain of IKKβ, strongly supporting the specificity of this interaction (Fig. 5a *lower panel* and Supplementary Fig. 5d). This finding is also in line with a previous study showing that a construct of the isolated SDD domain of IKKβ is sufficient for interaction with IκBα[11]. EDC/sulfo-NHS, a zero-length cross-linker catalyzing amide bond formation, provided 10 cross-links mostly involving Glu or Asp residues of the N-terminal acidic patch of IκBα pep and Lys residues of the dimerization region of IKKβ (Supplementary Fig. 5d *upper panel)*. Consistently, the long-range BS3 cross-linker identified 5 amine-to-amine links between the peptide's N-terminus and the same Lys residues (Supplementary Fig. 5d *middle panel)*, thereby confirming the proximity of the N-terminal acidic patch of IκBα pep to the IKKβ dimerization region. Sulfo-SDA, a short spacer (3.9 Å) cross-linker that conjugates primary amines or hydroxyls with any amino acid group after UV photoactivation[33], provided 26 links (Supplementary Fig. 5d *lower panel)*.

Topological analysis of the CLMS data using the DisVis tool[34] indicates that the volume accessible to IκBα pep for interaction with IKKβ is consistent with a binding interface, which involves the dimerization and middle regions of the two adjacent SDD domains of the IKK dimer (Fig. 5b *left panel*). Many of the identified cross-links map to IKKβ residues Lys467-Met468-Lys469 (Fig. 5a *lower panel*). Consistently, after careful inspection of the x-ray data we were able to identify a small lobe of extra electron density in the proximity of these residues in the 'closed' A-B homodimer (Supplementary Fig. 4b), which suggests that IκBα pep might be bound at this site but not entirely visible at this resolution.

In the next step, we calculated a model of the IKKβ/IκBα complex. Unbound IκBα pep appears to be mostly random coil in solution (Supplementary Fig. 6). This peptide was docked in an extended conformation to the IKKβ A-B homodimer crystal structure using CLMS-derived distance restraints and the HADDOCK software (Fig. 5b *right panel*). Eight acceptable clusters were obtained based on the HADDOCK score and interface root-mean-square deviation (RMSD) (Supplementary Fig. 7a). In all clusters, IκBα pep binds to the two adjacent SDD domains of the IKKβ homodimer, with the YDDΦxΦ motif accommodated in a groove contributed by helices α2s and α4s from protomer A, and α2s from protomer B of the SDD middle portions (Fig. 5b *right panel* and Supplementary Fig. 7b). Structural alignment of the models shows high precision for most of the clusters, with mean within-cluster interface RMSD values ranging between 1.3 and 1.8 Å. (Supplementary Fig. 7a). The best model from the cluster with the lowest HADDOCK score (cluster 1) is chosen as a representative model (Supplementary Data 1). Overall CLMS distance restraints are in good agreement with this final model (Supplementary Fig. 7c). Most over-length cross links involve flexible residues at the N-terminus of IκBα pep (Glu 297 and Phe298) and of the C-terminus of IKKβ (Lys659 and Lys 664), and likely reflect disorder and/or the capturing of transient oligomeric interactions (Supplementary Fig. 7c, d).

The YDDΦxΦ binding groove is dominated by polar and positively charged residues, with a few hydrophobic contributions observed in the proximity of the Y_1 (Tyr305), Φ_4, (Cys308) and Φ_6 (Phe310) positions of the motif (Fig. 5c). Specifically, whereas Tyr305 makes stacking interactions with Met475 of IKKβ, Cys308 and Phe310 are inserted in a cavity contributed by Ala473, Val530, Val534 and Met538 of the two adjacent SDD domains of IKKβ (Fig. 5c *left panel*). The acidic residues of the motif (Asp306 and Asp307) are instead stabilized by a positively charged patch comprising Lys467, Lys480 and Lys531 of IKKβ (Fig. 5c, *right panel*). Several residues lining the

https://doi.org/10.1038/s41467-024-52076-0

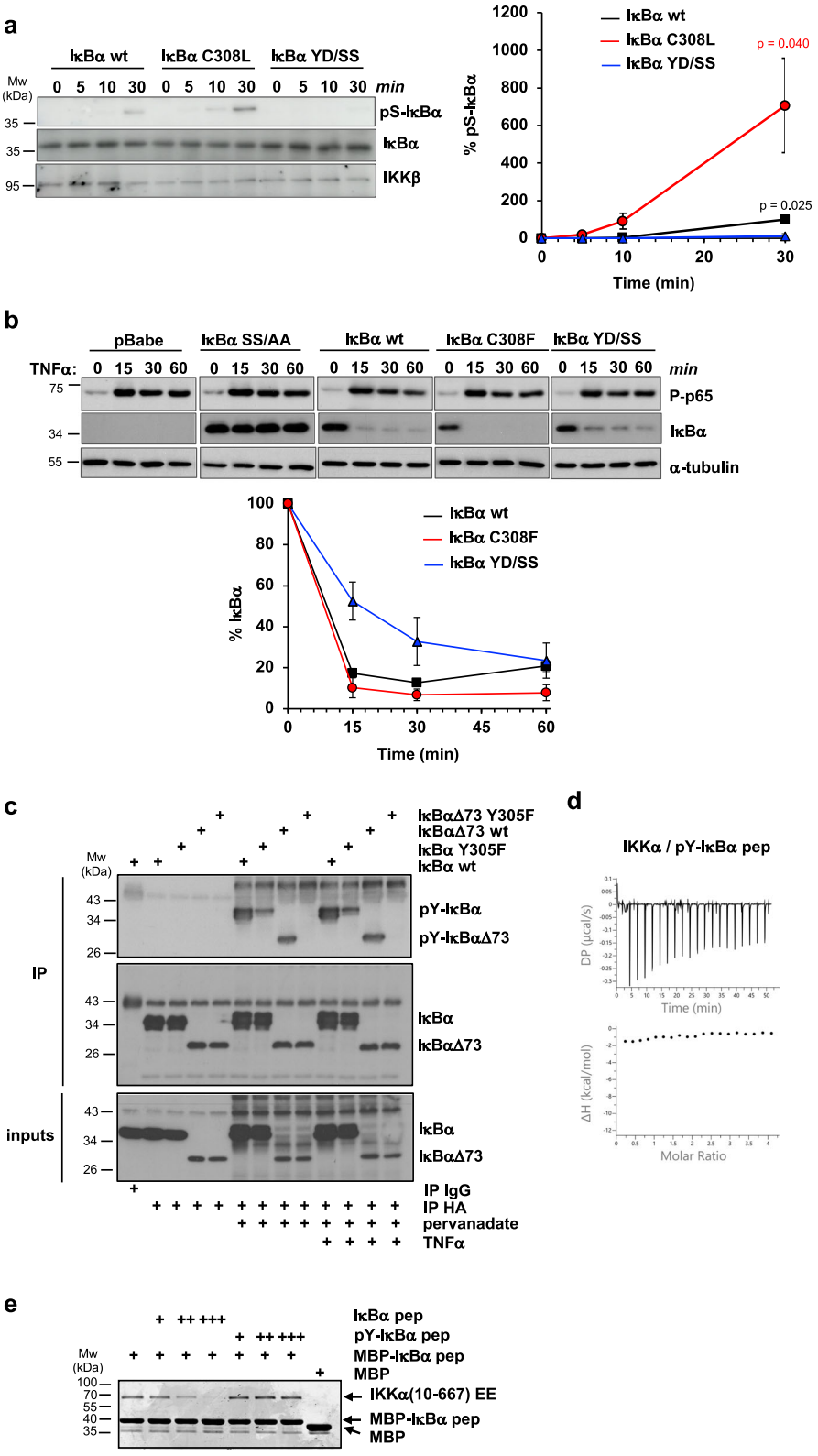

YDDΦxΦ groove are conserved across species in both IKKα and IKKβ, whereas the positively charged surface contacting the N-terminal acidic patch of the IκBα pep appears to be more variable (Supplementary Fig. 8).

Based on the structural model, we designed IKKβ mutants (Supplementary Fig. 9a) and evaluated their interactions with the IκBαΔ73 and IκBα pep(s) constructs by the GPCA and pulldown assays, respectively. Strikingly, the L654D/W655D mutation in the C-terminal portion of the SDD domain, previously reported to suppress IKKβ dimerization[12], completely abolishes binding to IκBα in both assays, thereby providing evidence that an intact dimer is required for the interaction with the substrate (Fig. 5d, e and Supplementary Fig. 9b, c). This is in line with previous results, showing that this mutation markedly reduces IKKβ-mediated phosphorylation of the IκBα substrate[12]. In addition, we also identified single amino acid substitutions introducing charge reversal (K469E and K480E) or affecting hydrophobicity

Fig. 3 | Functional analyzes on the YDDΦxΦ docking interaction. a In vitro kinase activity experiments using purified full-length 6xHis-IκBα proteins and endogenous IKK immunoprecipitated from HEK293T cells. Aliquots of the reactions were taken at the indicated time points and immunoblotted using anti-His (IκBα), anti-phospho-Ser32/Ser36 IκBα (pS-IκBα) and anti-IKKβ (IKKβ) antibodies. Samples were run on two separate 10% SDS-PAGE gels for detection of total IκBα and pS-IκBα. (*Left panel*) Representative Western blot images. (*Right panel*) Quantification of pS-IκBα levels normalized to IκBα at 30 min (100%). The data (mean +/− SD) are obtained from three independent kinase activity experiments. The indicated *P*-values (p) are obtained from a two-tailed unpaired *t*-test, $n = 3$ biological triplicates. Black: differences between IκBα YD/SS and IκBα wt; red: differences between IκBα C308L/F and IκBα YD/SS. **b** *In cellulo* degradation of retro-transduced IκBα proteins in MEF cells KO for IκBα, IκBβ, IκBε. Cells were stimulated with TNFα (20 ng/ml) and collected at the indicated time points. Cellular extracts were immunoblotted using anti-IκBα (IκBα) and phospho-specific p65 (P-p65) antibodies. IκBα SS/AA: IκBα S32A/S36A. (*Upper panel*) Western blot images. Each IκBα mutant was migrated together with wt IκBα on the same gel (see Source Data file). (*Lower panel*). Quantification of IκBα levels normalized first to tubulin and, then, to the IκBα values at time 0 (100%). The data (mean +/− SD) are obtained from three measurements, with bars reporting on the quantification error. Similar IκBα degradation profiles were obtained in a second independent experiment. **c** Detection of IκBα tyrosine phosphorylation in HEK293T cells. Cells were transfected with the indicated HA-tagged IκBα constructs, incubated, or not, with pervanadate (1 mM) for 30 min and stimulated, or not, with TNFα (10 ng/ml) for 15 minutes before collection. Cleared lysates were immunoprecipitated with anti-HA beads, and immunoblotted with anti-phospho-Tyr (pY-IκBα and pY-IκBαΔ73) and anti-HA (IκBα and IκBαΔ73) antibodies. The results were reproduced in a second independent experiment. **d** ITC data on the IKKα interaction with synthetic phospho-Tyr305 IκBα pep (pY-IκBα pep). **e** Competition MBP-pulldown experiment using 6xHis-IKKα(10-667) EE, MBP-IκBα pep coupled to amylose resin and an excess of synthetic IκBα pep or pY-IκBα pep peptides. IKKα : (pY-)IκBα pep stoichiometric ratios: 1:100 (+), 1:200 (+ +); 1:500 (+++). Samples were migrated on a 10% SDS-PAGE gel and stained by Coomassie. These results were reproduced in a second independent pulldown experiment. Source data for this figure are provided as a Source Data file.

(M475A) at specific positions of the YDDΦxΦ binding groove, which significantly attenuate the binding response to IκBα (Supplementary Fig. 9b, c). The combination of these substitutions in single constructs (K469E/K480E and K469E/M475A) leads to a stronger reduction of binding activity in both assays (Fig. 5d, e and Supplementary Fig. 9b, c). In contrast, the R460E mutation appears to reduce binding to IκBαΔ73 but not to the IκBα pep(s), suggesting that Arg460 may contribute to interactions involving IκBα residues outside the YDDΦxΦ motif (Fig. 5d, e and Supplementary Fig. 9b, c). Significant effects are also observed for charge reversal mutations within the C-terminal helix contacting the N-terminal patch of IκBα pep (K641E, R645E, K659E and K664E), suggesting that this interface may provide additional electrostatic contributions (Supplementary Fig. 9b, c).

Together the results described in this section indicate that the YDDΦxΦ motif interacts with a conserved groove at the interface of the IKKβ homodimer.

The YDDΦxΦ motif mediates IKK interactions with partner proteins in NF-κB signaling

Proteome-wide bioinformatic analyzes using SLiMSearch[35] detected 27 matches with an accessible YDDΦxΦ consensus (YDD[MILVCF].[-MILVCF]) (Supplementary Data 2). Among these matches we found three proteins annotated to bind to IKKα or IKKβ, namely: IκBβ, a canonical substrate of IKKβ and orthologue of IκBα; p100, the IKKα substrate in the alternative NF-κB pathway; and interferon regulatory factor 7 (IRF7), which was also reported to be a substrate of IKKα[24]. We thus designed peptides containing the YDDΦxΦ sequences from these proteins (referred to as IκBβ pep, p100 pep and IRF7 pep hereafter, Fig. 6a) and tested them against recombinant IKKα and IKKβ by pulldown (Fig. 6b). The results show that IKKβ binds uniquely to peptides derived from the catalytic IκB substrates (IκBα pep and IκBβ pep) and not to p100 pep or IRF7 pep. In contrast, all the peptides interact with IKKα.

The alternative p100 substrate consists of an N-terminal disordered region, followed by a Rel homology domain (RHD), an ankyrin repeat domain (ARD), a death domain (DD) and a disordered C-terminal region (Fig. 6c *left panel*). The YDDΦxΦ motif is located in the N-terminal disordered region and is conserved from human to fish (Fig. 6c *right panel*), whereas the IKKα phosphorylation sites are situated within the RHD and C-terminal regions[10]. Synthetic p100 pep binds to purified IKKα with an affinity (K_D) of approximately 12 μM, which is very similar to that of IκBα pep (Table 1 and Fig. 6d). In vivo GPCA analyzes show that deletion of the C-terminal region of p100 harboring some of the phospho-acceptor residues does not affect IKKα interaction with p100 (Fig. 6e, *left panel*, compare FL with 1-852). Instead, a double Ser substitution at the Y_1 and D_3 positions of the docking motif (i.e. YD/SS) or deletion of the motif strongly reduces binding to IKKα (Fig. 6e *left panel*, compare FL with FL YD/SS and 39-852).

In IRF7 the YDDΦxΦ motif is conserved in mammalian orthologues and lies within a C-terminal autoinhibitory domain (ID), just downstream of the serine cluster phosphorylated by the TBK1/IKKε kinase (Supplementary Fig. 10a, b)[36,37]. ITC measurements show that IRF7 pep binds with weak affinity to IKKα (Supplementary Fig. 10c). While we were able to reproduce IRF7 protein binding to IKKα in vivo by GPCA, such interaction is not affected by mutation of the Y_1 and D_3 motif positions (IRF7 YD/SS in Supplementary Fig. 10d). Since TBK1/IKKε phosphorylation of IRF7 induces major conformational changes in the ID domain of IRFs[38], which may enhance motif accessibility, we introduced phosphomimetic mutations in the serine cluster and tested the impact on the IKKα/IRF7 interaction (Supplementary Fig. 10b). The results show no effect of such mutations on the interaction (Supplementary Fig. 10d), suggesting that a mechanism other than TBK1/IKKε phosphorylation may be associated with motif regulation in IRF7.

We also designed peptides from seven other matches with an accessible motif and with a functional relation to cell signaling (Supplementary Data 2 and Supplementary Fig. 11a). Such peptides were tested for interaction with recombinant IKKα and IKKβ homodimers by pulldown. Only one peptide derived from the B-cell scaffold protein with ankyrin repeats (BANK1) is found to interact with IKKα, while no peptide interacts with IKKβ (Supplementary Fig. 11b). These results indicate that specific residue positions, *e.g.* the variable x of the motif or positions flanking the motif, are probably not compatible with certain amino acids. The sequence Logo derived from orthologous peptides from IκBα, IκBβ, p100, IRF7 and BANK1 is shown in Fig. 6h.

In BANK1 the YDDΦxΦ motif is conserved in mammalian orthologues and lies in the C-terminal region predicted to be disordered (Fig. 6f). Results from in vivo GPCA analyzes validate the interaction between the full-length IKKα and BANK1 proteins and further demonstrate the contribution of the motif since mutation of the Y_1 and D_3 positions (YD/SS) leads to a reduction of IKKα binding (Fig. 6g). Notably, BANK1 is expressed in B-cells and has been shown to function downstream of the BCR receptor and to associate to the NF-κB effectors TRAF6 and MyD88[39,40].

Taken together these results show that the YDDΦxΦ motif is required for docking of IKKα and IKKβ homo- and heterodimers to multiple partner proteins within the NF-κB compartment.

Discussion

Kinase-substrate interactions involving SLiM recognition are mediated by docking grooves either within the kinase domain, or in separate globular domains (*eg.* SH2, SH3) or in associated regulatory proteins

https://doi.org/10.1038/s41467-024-52076-0

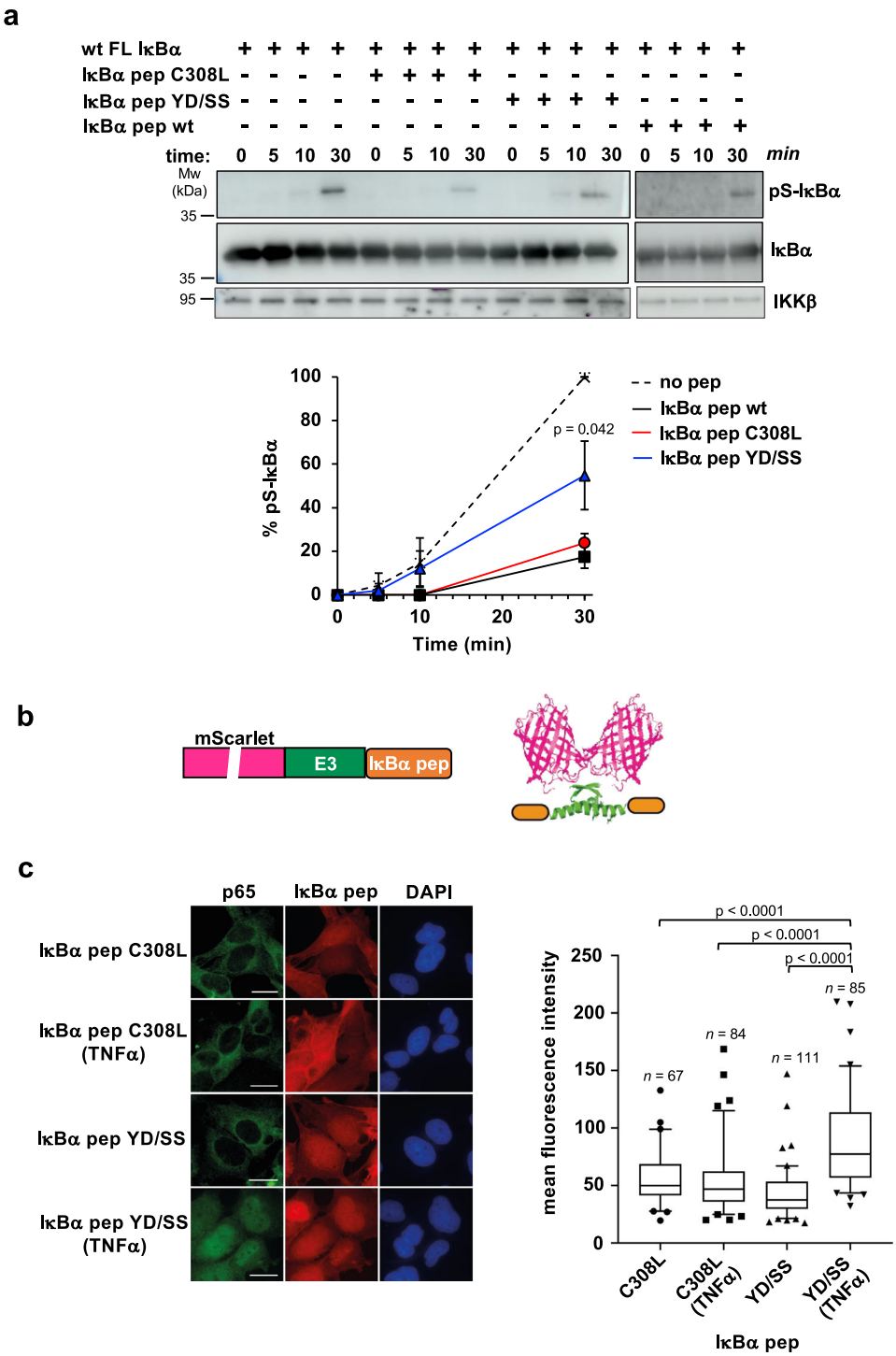

Fig. 4 | Inhibition of canonical NF-κB signaling by IκBα pep. a In vitro inhibition of IKKβ kinase activity by synthetic IκBα pep variants. The experiment uses full-length wt 6xHis-IκBα, endogenous IKK, and an excess of synthetic IκBα pep variants. Samples were run on two separate gels for detection of total IκBα and pS-IκBα. See also legend of Fig. 3a. (*Upper panel*) Representative Western blot images. All different IκBα pep conditions were migrated with the reference (no peptide) on the same gel (see Source Data file). (*Lower panel*) Quantification of IκBα phosphorylation levels normalized to the values obtained in the absence of peptide (no peptide) at 30 minutes incubation (100%). The data (mean +/− SD) are obtained from three independent kinase activity experiments. The indicated *P*-value (p) was obtained from a two-tailed unpaired *t*-test, $n = 3$ biological triplicates and reports on differences between IκBα pep YD/SS and IκBα pep wt at t = 30 min. **b** Schematic representation of mScarlet-E3-IκBα pep constructs. Purple: mScarlet, green: the E3 dimerization peptide; orange: the IκBα pep sequence. **c** In vivo inhibition of NF-κB signaling by IκBα pep. (*Left panel*) Immunofluorescent staining of MRC5 cells electroporated with mRNAs coding for mScarlet-E3-IκBα pep fusions. After electroporation, cells were treated or not with TNFα (20 ng/ml) for 30 minutes before fixation. The translated constructs were detected by direct immunofluorescence of the mScarlet (red). p65 was detected using an anti-p65 antibody followed by an anti-mouse Alexa-Fluor 488 (green). Nuclei were stained by DAPI. Scale bar, 10 µm. (*Right panel*) Mean fluorescence intensities of nuclear p65 in the four conditions. The data are displayed in a box-and-whisker representation showing the median in the center line, the 75/25 percentiles at the boxes, the 5/95 percentiles at the whiskers and the extreme values to the minimum and maximum of the raw fluorescence data. Statistical analysis was performed by ordinary one-way ANOVA test. *n*: number of cells analyzed. See also Supplementary Fig. 3b for quantification of the nuclear expression levels of IκBα pep fusions. Source data for this figure are provided as a Source Data file.

https://doi.org/10.1038/s41467-024-52076-0

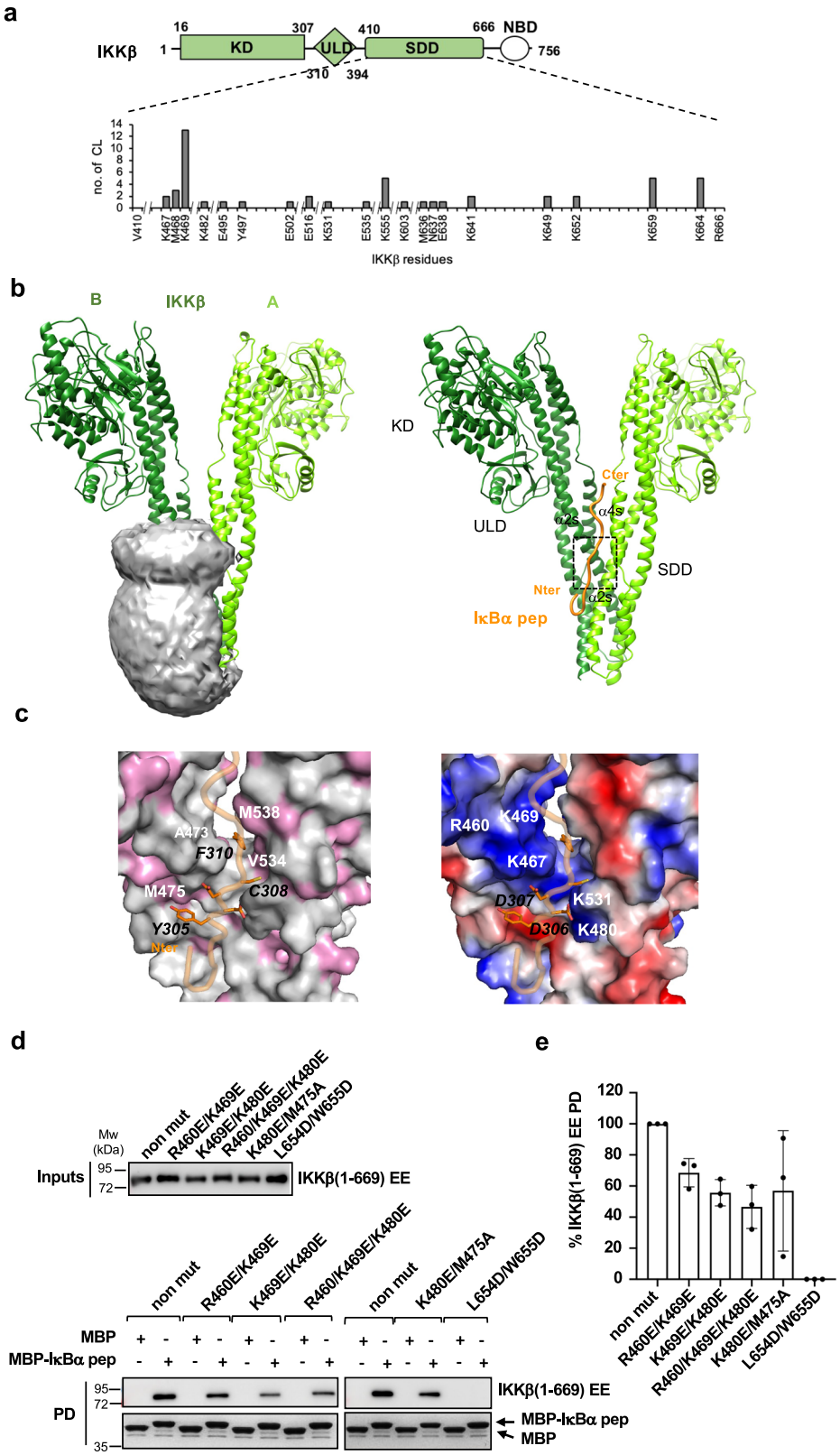

(*e.g.* cyclins)[28]. In this work, we show that IKKs have developed an alternative mechanism, which relies on a docking groove generated by dimerization of the SDD domain and which is negatively regulated by SLiM phosphorylation. Since dimerization is also required for kinase activation through the formation of higher order oligomers[12], it appears that the SDD domain has evolved as a versatile structure, which ensures kinase activation and, at the same time, interaction with the substrate. This domain is also present in the IKK-related kinases TBK1 and IKKε, where it mediates dimerization and kinase activation via *trans*-autophosphorylation[41]. However, we did not detect any significant interaction between TBK1 or IKKε and the YDDΦxΦ motif peptides investigated in this work (Supplementary Fig. 12), suggesting that this motif is specific for dimers of IKKα and IKKβ. The IKK docking mechanism described here is reminiscent of the

Fig. 5 | Structural analyzes of the IKKβ/IκBα pep interaction. a (*Upper panel*) Architecture of IKKβ. Green: KD, ULD and SDD domains present in the IKKβ(1-669) EE construct; white NEMO binding domain (NBD). (*Lower panel*) SDD residues involved in cross-links (CL) with the IκBα pep peptide. Y axis: total number of links obtained with the three cross-linkers (EDC/NHS, BS3 and sulfo-SDA). **b** (*Left panel*) The volume accessible to IκBα pep for interaction with IKKβ calculated using the CLMS data and the DisVis program[34]. The gray mesh indicates the center-of-mass position of IκBα pep, while protomers A and B of the IKKβ dimer crystal structure are shown in the ribbon representation in light and dark green, respectively. (*Right panel*) Best model of the IKKβ/IκBα pep complex obtained using the x-ray A-B IKKβ dimer structure and CLMS derived distance restraints for docking of IκBα pep (orange). The dashed box positions the YDDΦxΦ motif. Images were made using the UCSF Chimera software[74]. **c** Molecular views of the complex interface showing IKKβ and IκBα pep in the surface and ribbon representation, respectively. Side-chains of conserved YDDΦxΦ residues are displayed and indicated by black labels. IKKβ interface residues are indicated by white labels. (*Left panel*) Surface hydrophobic residues of IKKβ (pink). (*Right panel*) Surface charge potential of IKKβ. Blue: positive charge; red: negative charge. **d** Pulldown analyzes of the interactions between recombinant purified IKKβ mutants and MBP-IκBα pep(s). non mut: 6xHis-IKKβ(1-669) EE without additional mutations. (*Upper and lower panels*) Representative gel images. IKKβ proteins were detected by Western blot (anti-His antibody), while MBP-IκBα pep(s) by Coomassie staining. See also legend of Fig. 1b. **e** Quantification of pulldown analyzes. The IKKβ band intensities were normalized to 100% for the reference protein (i.e. non mut IKKβ). The data (mean +/− SD) are derived from three independent experiments ($n = 3$). Source data for this figure are provided as a Source Data file.

mode of action of the protein kinase A (PKA) holoenzyme, which uses dimerization of the DD domain of the PKA regulatory subunit (PKA-R) to generate a hydrophobic groove that targets helical motifs of AKAP proteins[42,43].

Here we show that the affinity of the docking interaction correlates with phosphorylation of the IκBα substrate. This result is in agreement with early reports on the higher catalytic efficiencies of IKKβ homo- and heterodimers for the full-length IκBα protein comprising the YDDΦxΦ motif as compared to an N-terminal IκBα peptide encompassing the phosphorylation site[44–46]. Remarkably, these studies report that catalytic efficiency is the highest in the case of the IKKα/IKKβ heterodimer, a finding which could be explained by the higher binding affinity of IKKα for the docking motif as compared to IKKβ. Together, these results indicate that, in addition to mediating IKKβ activation and p100 phosphorylation, IKKα provides substrate recruitment functions in NF-κB signaling.

Upon stimulation of canonical NF-κB signaling, phosphorylation of IκB proteins occurs much more efficiently and rapidly as compared to other substrates such as p65 and p105, or of p100 after stimulation of the alternative pathway[47]. Such a fast response is primarily mediated by the scaffolding function of NEMO, which interacts with both IKK dimers via its N-terminus and with IκBs via its C-terminal zinc-finger domain, thereby channeling IKK activity specifically to IκBs[15]. From this, it appears that canonical IKK may use at least two interfaces to interact with IκBs, i.e. the YDDΦXΦ docking groove and the NEMO zinc finger (Fig. 7). Whether these interfaces co-exist in a single IKK/NEMO-IκB complex or whether different conformational states of the complex exist remains to be determined. Interestingly, Hoffmann and coworkers report that the NEMO-IκBα interaction is strengthened by IKKβ, an observation that would be in favor of co-existence of multiple interfaces[15].

Here, we find that the YDDΦxΦ motif also mediates p100 recruitment to the IKKα homodimer. In a previous study, Xiao et al. found that the NIK kinase associated to the 'alternative' IKK complex interacts with p100[10]. Hence, the overall picture which emerges from this and previous studies is that IKK complexes acting in NF-κB signaling use multiple binding interfaces, which are contributed by both catalytic dimers and regulatory subunits (Fig. 7).

To the best of our knowledge, the YDDΦxΦ consensus has not been previously reported for a SLiM. This consensus is conserved in NF-κB substrates (IκB and p100) from humans to fish. We find that phosphorylation at the strictly conserved Y_1 position occurs in IκBα at steady state and has a detrimental effect on the binding to IKK dimers. These results are in line with previous work showing that phosphorylation at this position in IκBα increases upon activation of the c-Abl kinase by genotoxic stress[30], and that this is associated with IκBα accumulation and inhibition of expression of NF-κB-dependent cell survival genes[30,48]. Together, these findings suggest that Tyr305 phosphorylation may represent a critical point of regulation by signaling pathways converging at the canonical IKK-IκBα complex.

The YDDΦxΦ motif is also conserved in IRF7, a known substrate of IKKα. However, although an IRF7 peptide binds weakly to IKKα in vitro, our analyzes failed to demonstrate a significant contribution of the motif towards the IKKα/IRF7 interaction in vivo. Based on YDDΦxΦ motif predictions, we identified BANK1 as a partner of IKKα. BANK1 is a scaffold protein expressed in B-cells, first described to function downstream of the BCR receptor to promote Ca^{2+} mobilization from intracellular stores[39] and, more recently, reported to associate to TRAF6 and MyD88, two major NF-κB effectors in immune cells[39,40]. Elucidation of the function of the IKK/BANK1 interaction, i.e. substrate phosphorylation or anchoring of IKK to receptor-associated complexes, will be the subject of future studies.

IKKs have been reported to interact with a large number of substrates involved in several signaling pathways[23]. Yet, so far, only effectors of NF-κB signaling seem to interact with IKK dimers via the YDDΦxΦ motif. Thus, we expect that, just like in the case of MAPK kinases[49], variations of the YDDΦxΦ consensus would still be recognized by the docking groove identified in this work. Given the lack of high-resolution reporting on side-chain conformation, it is difficult to predict such variations. In addition, IKK dimers may also encompass other docking grooves/pockets, which target completely unrelated SLiMs, similarly, to Protein Ser/Thr phosphatase-1 (PP1), which has developed distinct binding pockets dedicated to the different motifs of PP1-interacting proteins (PPI)[50]. Future proteome-wide analyzes combined with structural studies will provide a global view on the protein-protein interaction mechanisms used by IKKs to selectively recruit their substrates.

Deregulation of NF-κB signaling occurs in many pathologies, including infectious, inflammatory, and autoimmune diseases, and cancer. Since enzymatic inhibitors of IKKβ have been associated with serious side effects[51], peptide inhibitors derived from the NEMO subunit have been proposed as alternative therapeutic approaches[52,53]. Here, we show that a bivalent peptide derived from the YDDΦxΦ motif of IκBα efficiently inhibits canonical NF-κB signaling. It is tempting to speculate that, in addition to inhibiting interactions with the substrate, the bivalent peptide may also reduce kinase activation, by constraining the IKK dimer in a closed conformation and, thus, preventing IKK dimer oligomerization or secondary interface IKK-NEMO interactions[54]. Further structural analyzes will be required to evaluate this hypothesis.

To conclude, this work unveils the mechanism of substrate docking to IKK catalytic dimers. This mechanism, which is conserved in both the 'canonical' and 'alternative' branches of NF-κB signaling, probably conveys an upper level of recognition, with fine tuning of substrate specificity and/or kinetics being achieved through regulatory proteins of IKK complexes.

Methods

Details of reagents used in this study are provided in Supplementary Data 3.

https://doi.org/10.1038/s41467-024-52076-0

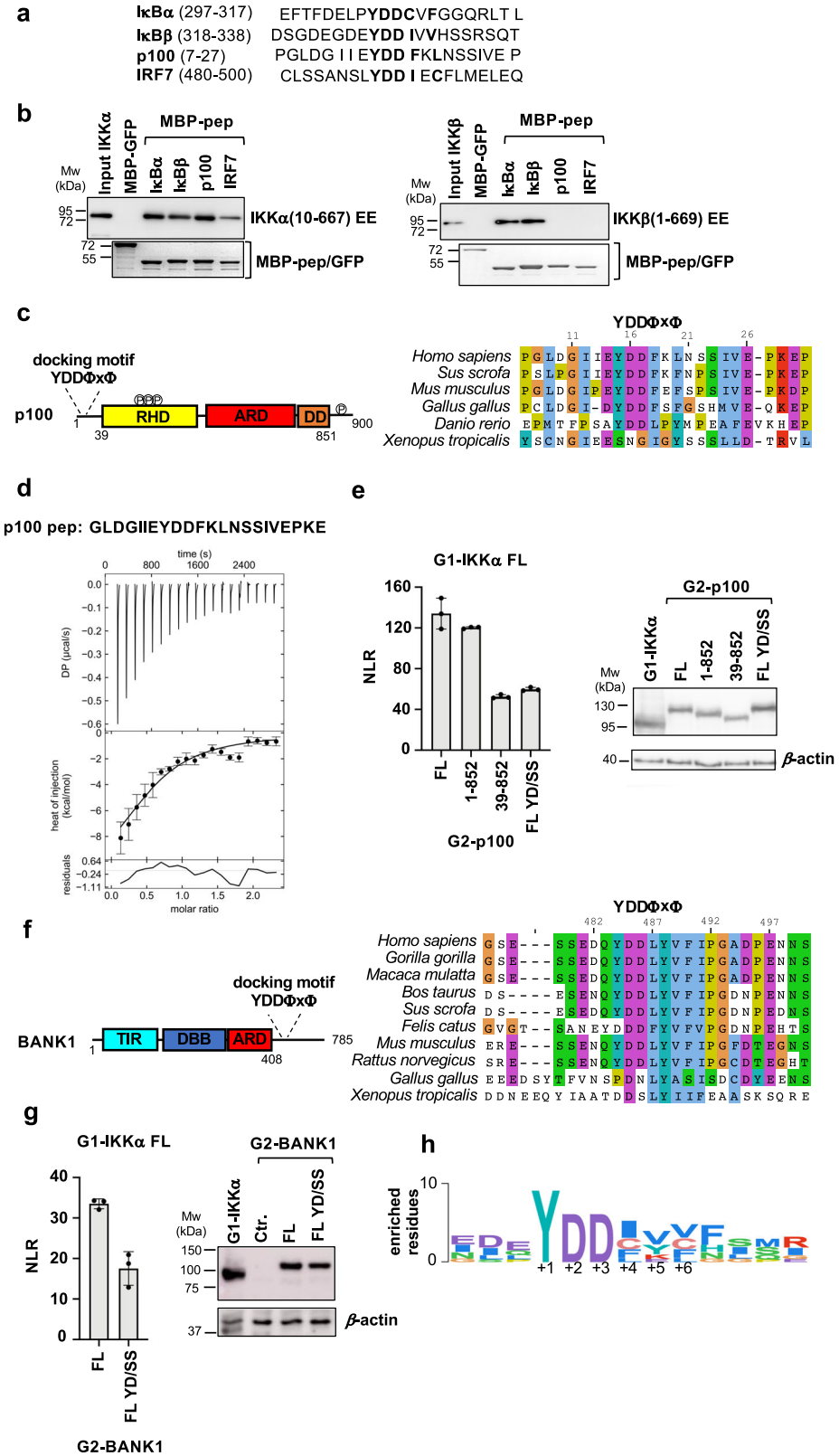

DNA constructs

Expression in E. coli and insect cells. Full-length and deletion constructs of IκBα for *E. coli* expression were amplified by PCR and cloned into the NcoI and BamH1 sites of a modified pETM-41 and/or pETM10 vectors (kindly provided by G. Stier, University of Heidelberg), allowing for expression of N-terminal MBP and 6xHis tags, respectively. MBP-peptide fusions were obtained by ligation of complementary oligonucleotides coding for the peptide sequence into the NcoI and BamH1 sites of the modified pETM-41 vector.

The IKKβ(1-669) S177E/S181E (i.e. IKKβ(1-669) EE) and the IKKα(10-667) S176E/S180E (IKKα(10-667) EE) constructs for baculovirus expression were amplified by PCR and inserted by Gateway cloning into modified pBacPAK8 vectors, thereby allowing for expression of N-terminal 6xHis or Strep tags followed by a TEV protease cleavage site.

Fig. 6 | The YDDΦxΦ motif in NF-κB signaling partners of IKKs. a Motif peptide sequences from *human* IκBα, IκBβ, p100 and IRF7 proteins used in the pulldown experiments shown in (**b**). **b** Pulldown analyzes of the interactions between recombinant 6xHis-IKKα(10-667) EE (*left panel*) or 6xHis-IKKβ(1-669) EE (*right panel*) proteins and MBP-peptide fusions. IKKα and IKKβ were detected by Western blot (anti-His antibody) and MBP-peptides by Coomassie staining. These results were reproduced in at least two independent pulldown experiments. See also legend of Fig. 1b. **c** (*Left panel*) Domain architecture of p100. Disordered N-terminal region containing the YDDΦxΦ motif; RHD: Rel homology domain (residues 38-343) containing IKKα phosphorylation sites; ARD: ankyrin repeat domain (residues 487-758); DD: death domain (residues 764-851); disordered C-terminal region containing IKKα phosphorylation sites. (*Right panel*) Sequence alignment of residues 7-30 of *human* p100 showing conservation of the YDDΦxΦ motif. **d** Representative ITC binding isotherm for the IKKα/p100 pep interaction. The sequence of the synthetic p100 pep peptide is reported at the top. The data were analyzed by global fitting (see Table 1). The interaction was measured in two independent ITC titrations. Error bars correspond to the RMSD of the fitted curve and experimental values. See also legend of Fig. 2. **e** (*Left panel*) Representative dataset for the GPCA analysis of the interactions between full-length wt G1-IKKα and G2-p100 proteins. G2-p100 FL YD/SS: G2-p100 FL Y15S/D17S. (*Right panel*) Expression levels of G1-IKKα and G2-p100 constructs in HEK293T cells. See also legend of Fig. 1d. **f** (*Left panel*) Domain architecture of BANK1. TIR: Toll/interleukin-1 receptor/resistance protein domain (residues 25-153); DBB: Dof/BCAP/BANK domain (residues 200-327); ARD: ankyrin repeat domain (residues 342-408); disordered C-terminal region containing the YDDΦxΦ motif. (*Right panel*) Sequence alignment of residues 475-500 of *human* BANK showing conservation of the YDDΦxΦ motif in mammalian orthologs. **g** (*Left panel*) Representative dataset for the GPCA analysis of the interactions between full-length wt G1-IKKα and G2-BANK1 proteins. G2-BANK1 FL YD/SS: G2-BANK1 FL Y484S/D486S. (*Right panel*) Expression levels of G1-IKKα and G2-BANK1 constructs in HEK293T cells. Ctr.: non transfected cells. See also legend of Fig. 1d. **h** Sequence Logo showing the position-specific frequency of amino acids composing the motif in orthologues of IκBα, IκBβ, p100, IRF7 and BANK1. The Logo is based on the PSSM created using the binomial $\log_{10}$ scoring scheme from PSSMSearch (https://slim.icr.ac.uk/pssmsearch/) for the five validated peptides. Source data for this figure are provided as a Source Data file.

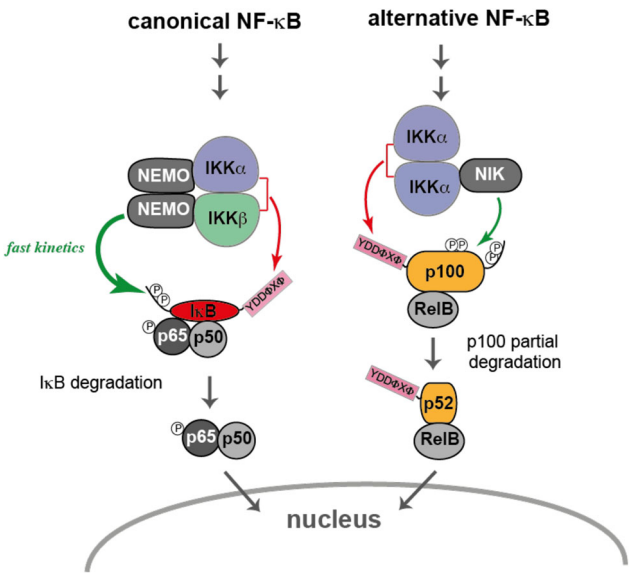

Fig. 7 | Illustration of known protein-protein interactions mediating substrate recruitment to IKK complexes in NF-κB signaling. Red arrows: interactions involving YDDΦxΦ docking to catalytic dimers; green arrows: interactions involving regulatory subunits.

Expression in mammalian cells. Full-length IKKα, IKKβ, IκBα, p100, IRF7, BANK1, and constructs of these proteins used in the GPCA experiments were amplified by PCR and inserted into the pSPICA-N1 and pSPICA-N2 (both derived from the pCiNeo mammalian expression vector and kindly provided by Y. Jacob, Institut Pasteur, Paris) by Gateway cloning. These vectors enable expression of the Gluc1 (pSPICA-N1) and Gluc2 (pSPICA-N2) complementary fragments of the *Gaussia princeps* luciferase, which are linked to the N-terminal ends of the tested proteins by a flexible 20 amino acid linker[55]. Full-length wt and mutant IκBα constructs for virus preparation were cloned in the EcoRI and BamHI sites of the pBABE-puro retroviral vector[56]. To generate the mScarlet-E3-IκBα pep fusions, the DNA sequences coding for the E3 peptide[31] fused to the IκBα pep variants were synthetized by Integrated DNA Technologies and cloned into the NheI and EcoRI sites of a pET vector allowing for the expression of a N-terminal mScarlet tag.

Mutagenesis. Side-directed mutagenesis of IKKα, IKKβ, IκBα, p100, IRF7, and BANK1 was performed using the QuickChange II kit (Agilent). ORFs coding for IKKα, IKKβ, IκBα, p100, and IRF7 were obtained from Addgene. The ORF of BANK1 from DNASU. All constructs were verified by DNA sequencing.

Virus production

The recombinant viruses (bacmid) for expression in insect cells were generated by co-transfection of *Spodoptera frugiperda* Sf9 insect cells (Oxford Expression Technologies) grown in Grace insect medium (Gibco) supplemented with 10% FCS (Gibco)[57]. Briefly, 250 ng of linearized AcMNPV BAC10:KO1629, Δv-cath/chiA, mCherry bacmid[57] and 750 ng of pBacPAK8 vectors containing the IKKα(10-667) EE or IKKβ(1-669) EE inserts were transfected into Sf9 cells using lipofectamine 2000 (Invitrogen) in a T25 flask. Viruses contained in the medium after one-week incubation at 27 °C were subjected to a round of amplification yielding the P1 virus stock.

Viruses used for MEF transduction were obtained by transfecting Phoenix-eco cells (5×10^6) with 6 µg of pBABE-IκBα plasmid (empty vector was used as control) and 12 µl of TransIT (Mirus) as a transfection reagent. The medium was changed after 6 hours and replaced with 8 ml of fresh medium. The medium with virus was collected after 48 hours, filtered and used to infect MEFs.

Cell culture and transfection

Spodoptera frugiperda Sf9 cells used to generate and amplify viruses were grown in Grace medium supplemented with 10% FCS (Gibco), whereas Sf21 cells (Oxford Expression Technologies) for expression in insect cells were grown in the serum-free medium (Gibco). HEK293T were cultured in Dulbecco's modified Eagle's medium (DMEM), supplemented with 10% FCS at 37 °C with 5% CO_2 and transfected using JetPEI® (Polyplus transfection). MEFs KO for IκBα, IκBβ, IκBε (kindly provided by Alexander Hoffmann, UCLA) were cultured in DMEM supplemented with 10% FCS and Pen-strep. Supernatants containing viruses (see above) were added to 2×10^6 MEF cells with polybrene (4 µg/ml) overnight. The medium was subsequently changed with some fresh growing medium. MRC5 cells were cultured in DMEM supplemented with 4.5 g/L glucose, 10% FCS and 1 mM pyruvate.

Protein expression

E. coli. MBP-IκBα, MBP-peptide and 6xHis-IκBα fusion constructs for pulldown and in vitro activity assays were expressed in *E. coli* BL21 (DE3) cells. Cultures were grown at 37 °C until an optical density of 0.2–0.6 at 600 nm. The cultures were then incubated overnight at 18 °C. Cells were harvested and flash frozen in liquid nitrogen.

Insect cells. For production of 6xHis-IKKα(10-667) EE and 6xHis-IKKβ(1-669) EE homodimer samples, Sf21 cells grown in suspension

were infected with the corresponding virus, harvested after 3 days incubation at 27 °C, washed in PBS containing 10% v/v glycerol and flash frozen in liquid nitrogen. Typically, cells are grown in 2 L flasks containing 500 ml of medium and are infected at a density of 1.10^6 cells/ml using 20 ml of P1 virus stock (assuming a titer of 5×10^7 pfu/ml, it corresponds to a multiplicity of infection of 2). For production of the IKKα/β heterodimer, Sf21 cells were co-infected with Strep-IKKα(10-667) EE and 6xHis-IKKβ(1-669) EE viruses. Cells were typically infected at a density of 2.10^6 cells/ml with a nominal multiplicity of infection of 0.5 for each virus (10 ml of each P1 virus stock for a 500 ml culture).

Protein purification

IKKα and IKKβ homodimers. Purification of 6xHis- IKKα(10-667) EE and 6xHis-IKKβ(1-669) EE constructs was carried out as previously reported[12,13], with modifications according to the specific use of the samples. Briefly, SF21 cells expressing IKKα or IKKβ proteins were resuspended in lysis buffer (25 mM Tris-HCl pH 8.0, 200 mM NaCl, 10 mM imidazole, 10% glycerol, 2 mM DTT, 1 µg/ml DNaseI, 0.2 µg/ml RNase, Roche complete™ protease inhibitor cocktail) and lysed by mild sonication. Lysates were centrifuged at 14500 *g* for 45 minutes at 4 °C. The supernatants were applied by gravity flow to Ni^{2+}-NTA agarose resin (Qiagen) pre-equilibrated in wash buffer 1 (25 mM Tris-HCl pH 8, 200 mM NaCl, 10 mM imidazole, 10% glycerol, 2 mM DTT). The resin was extensively washed by four consecutive steps using the following buffers: (i) wash buffer 1, (ii) wash buffer 2 (25 mM Tris-HCl pH 8, 200 mM NaCl, 25 mM imidazole, 10% glycerol, 2 mM DTT), (iii) wash buffer 3 (25 mM Tris-HCl pH 8, 1 M NaCl, 10% glycerol, 2 mM DTT) and (iv) wash buffer 1. IKKα or IKKβ proteins were eluted using elution buffer (25 mM Tris-HCl pH 8, 150 mM NaCl, 5% glycerol, 250 mM imidazole, 2 mM DTT).

In the case of IKKα and IKKβ proteins to be used for pulldown and kinase activity assays, samples were concentrated and incubated in the presence of 1 mM ATP plus additives (20 mM $MgCl_2$, 20 mM β-glycerophosphate, 10 mM NaF, and 1 mM sodium orthovanadate) for 1 hour on ice. Samples were then purified by gel filtration chromatography using a Superdex® 200 10/30 column (Cytiva) pre-equilibrated in gel filtration buffer 1 (20 mM Tris-HCl pH 8.0, 150 mM NaCl, 5% Glycerol, 2 mM DTT). In the case of cross-linking mass spectrometry experiments, concentrated IKKβ samples were incubated with a 20-fold excess of ML120B inhibitor (Sigma) plus additives for 1 hour on ice and then loaded on the Superdex® 200 10/30 column (Cytiva) pre-equilibrated in gel filtration buffer 2 (20 mM HEPES, pH 8.0, 150 mM NaCl, 5% glycerol, and 1 mM TCEP).

For the ITC and crystallization experiments, after the Ni^{2+}-NTA step the 6xHis tag was removed from the IKKα and/or IKKβ constructs by overnight digestion with TEV protease at the same time as dialysis against 20 mM Tris-HCl pH 8, 150 mM NaCl, 2 mM DTT, 5% glycerol. Then, the sample was applied to Ni^{2+}-NTA resin pre-equilibrated in dialysis buffer and the flow-through containing the IKKα or IKKβ protein collected. Next, the samples were concentrated, incubated with ML120B inhibitor plus additives for 1 hour on ice and was applied to a Superdex® 200 16/60 column (Cytiva) pre-equilibrated in gel filtration buffer 2 (20 mM HEPES pH 8.0, 250 mM NaCl, 2 mM TCEP). Finally, fractions containing the IKKα or IKKβ proteins were pooled together and the NaCl concentration adjusted to 150 mM. Purified IKKα and IKKβ samples were stored at 4 °C for up to 5 days.

IKKα/β heterodimer. SF21 cells expressing the Strep-IKKα(10-667) EE and 6xHis-IKKβ(1-669) EE proteins were resuspended in lysis buffer (100 mM Tris-HCl pH 8.0, 150 mM NaCl, 10% glycerol, 2 mM DTT, 1 µg/ml DNaseI, 0.2 µg/ml RNase, Roche cOmplete™ protease inhibitor cocktail) and lysed by mild sonication. Lysates were centrifuged at 14 500 *g* for 45 minutes at 4 °C. The supernatants were applied by gravity flow to Strep-Tactin XT 4 F resin (IBA-lifesciences) pre-equilibrated in wash buffer (100 mM Tris-HCl pH 8, 150 mM NaCl, 10% glycerol, 1 mM EDTA, and 2 mM DTT). After extensive washing the proteins were eluted with elution buffer (100 mM Tris-HCl pH 8, 150 mM NaCl, 10% glycerol, 2 mM DTT, and 50 mM biotin). The eluate was then applied to Ni^{2+}-NTA resin, which was washed and eluted as described above for the IKK homodimers. IKKα/β heterodimer samples were then concentrated and incubated in the presence of 1 mM ATP plus additives (see above) for 1 hour on ice. Finally, samples were purified by gel filtration chromatography using a Superdex® 200 10/30 column (Cytiva) pre-equilibrated in gel filtration buffer 1 (20 mM Tris-HCl pH 8.0, 150 mM NaCl, 5% Glycerol, 2 mM DTT).

6xHis-IκBα. BL21 cells expressing 6xHis-IκBα proteins for kinase activity studies were resuspended in 50 ml of lysis buffer (25 mM Tris-HCl pH 8, 250 mM NaCl, 10 mM imidazole, 5% glycerol, 0.2 % NP40, 2 mM DTT, 1 µg/ml DNase I, 0.2 µg/ml RNase, Roche cOmplete™ protease inhibitor cocktail) and lysed by sonication. Lysates were clarified by centrifugation at 96 000 *g* for 45 minutes at 4 °C. The supernatant was applied by gravity flow to Ni^{2+}-NTA agarose resin pre-equilibrated in wash buffer 1 (25 mM Tris-HCl pH 8, 200 mM NaCl, 10 mM imidazole, 2 mM DTT). The resin was washed with: (i) wash buffer 1, (ii) wash buffer 2 (25 mM Tris-HCl pH 8, 200 mM NaCl, 25 mM imidazole, 2 mM DTT), (iii) wash buffer 3 (25 mM Tris-HCl pH 8, 1 M NaCl, 2 mM DTT) and (iv) wash buffer 1. Subsequently, 6xHis-IκBα proteins were eluted with elution buffer (25 mM Tris-HCl pH 8, 200 mM NaCl, 250 mM imidazole, 2 mM DTT). Finally, imidazole was eliminated using a PD-10 desalting column (Cytiva) equilibrated in assay buffer (20 mM Tris-HCl, 150 mM NaCl, 2 mM DTT). Samples were concentrated, flash frozen in liquid nitrogen and stored at −80 °C.

MBP-fusions. For pulldowns, MBP-IκBα and MBP-peptide constructs were coupled to the amylose resin. Pellets of 10–25 ml of bacterial culture were resuspended in 2.5 ml of lysis buffer (20 mM Tris-HCl pH 8, 250 mM NaCl, 10% glycerol, 0.2 % NP40, 2 mM DTT, 1 µg/ml DNase I, 0.2 µg/ml RNase, Roche cOmplete™ protease inhibitor cocktail) and lysed by sonication. Lysates were centrifugated using a benchtop centrifuge at maximal speed and at 4 °C. Clarified lysates were incubated with 100 µl (dry bead volume) of previously equilibrated amylose resin (New England Biolabs) for 45 minutes at 4 °C on a rotating wheel. Resins were washed first with wash buffer 1 (20 mM Tris-HCl pH 8, 250 mM NaCl and 2 mM DTT) and then with wash assay buffer (20 mM Tris-HCl pH 8, 150 mM NaCl and 2 mM DTT). Resins coupled to MBP-fusion constructs were stored at 4 °C up to one week.

Chemical peptide synthesis

The synthesized peptides have the sequences reported below.

IκBα pep (residues 297-317 of IκBα): EFTEDELPYDDCVFGGQRLTL

C308L IκBα pep: EFTEDELPYDDLVFGGQRLTL

pY-IκBα pep: EFTEDELPpYDDLVFGGQRLTL

YD/SS IκBα pep: EFTEDELPSDSCVFGGQKLTL

C308L/R314K IκBα pep: EFTEDELPYDDLVFGGQKLTL

C308L/R314K IκBα-biot pep EFTEDELPYDDLVFGGQKLTLGGG-$(PEG)_3$-K-biotin

p100 pep (residues 8-29 of p100): GLDGIIEYDDFKLNSSIVEPKE

IRF7 pep (residues 495-516 of IRF7 isoform D): LSSANSLY DDIECFLMELEQPA

IκBα pep, pY-IκBα pep and p100 pep peptides were prepared by Fmoc/tBu-solid phase peptide synthesis (SPPS)[58] with the help of an ABI 433 A automatic peptide synthesizer in the form of C^{α}-carboxylates using preloaded resins (Novabiochem). C308L IκBα pep was assembled by Fmoc/tBu-SPPS using a CEM Liberty Blue microwave-assisted synthesizer in the form of C^{α}-amide (Rink-amide resin from Iris Biotech). YD/SS IκBα pep, C308L/R314K IκBα pep, C308L/R314K IκBα-biot pep and IRF7 pep were prepared by manual 'in situ neutralization' manual Boc/Bzl-SPPS[59] using MBHA-resin (Iris Biotech) as C^{α}-amides. IRF7 pep was acetylated at N-terminus. Standard protocols and

commercial amino acid building blocks were used in each case. Purification was carried out by reverse-phase HPLC (C18 column). Purity was controlled by analytical HPLC (> 95%) and masses were confirmed by LC-MS using electrospray ionization (ESI).

MBP-pulldown

Experiments were performed in PD buffer (20 mM Tris pH 8.0, 150 mM NaCl, 2 mM DTT). For each experiment, 10 µl of amylose resin (dry bead volume) coupled to MBP-fusion constructs were incubated with 500 µl of purified 6xHis-IKKα(10-667) EE or 6xHis-IKKβ (1-669) EE adjusted to a concentration of 0.4 µM for 2 hours at 4 °C. In the case of competition PD experiments, IKK samples were pre-incubated with an excess of synthetic IκBα pep peptides for one hour on ice. After two quick washing steps with PD buffer, complexes were eluted by incubation with 20 µl of the same buffer supplemented with 20 mM maltose for 15 minutes at 4 °C. After mild centrifugation, supernatants were recovered and migrated onto two separate 10% SDS-PAGE gels. One gel was used for Western blot analysis to detect His-IKKα or His-IKKβ using and anti-6xHis antibody (Sigma), the other for Coomassie staining to detect MBP-fusion proteins. Quantification of band intensity was done using the Image J software.

GPCA

HEK293T cells were transfected using the reverse transfection method. Transfection mixes containing 100 ng of pSPICA-N2 and 100 ng of pSPICA-N1 plasmids expressing test proteins plus PEI-MAX (Polysciences) were dispensed in white 96-well plates. HEK293T cells were then seeded on the DNA mixes at a concentration of 4.2×10^4 cells per well. 48 hours after transfection, cells were washed with 50 µl of PBS and lysed with 40 µl of *Renilla* lysis buffer (Promega) for 30 minutes with agitation. *Gaussia princeps* luciferase enzymatic activity was measured using a Berthold Centro LB960 luminometer by injecting 50 µl per well of luciferase substrate reagent (Promega) and counting luminescence for 10 seconds. Results are expressed as a fold change normalized over the sum of controls, specified herein as normalized luminescence ratio (NLR)[55]. For a given protein pair A/B, NLR = (Gluc1-A + Gluc2-B) / [(Gluc1-A + Gluc2) + (Gluc1 + Gluc2-B)]. In each GPCA dataset interactions were measured in three independent transfection experiments.

The expression levels of Gluc1- and Gluc2-fused proteins were checked by Western blotting. At 24 h post-transfection cells were collected, lysed by incubation on ice with lysis buffer (50 mM Tris pH 7.5, 150 mM NaCl, 1 mM EDTA, 1% Triton, cOmplete™ protease inhibitor) and centrifuged. Aliquots of cleared supernatants were loaded onto an 10% SDS-PAGE gel. Proteins were detected using a polyclonal antibody against the *Gaussia P.* luciferase (New England Biolabs or Invitrogen).

ITC

All experiments were performed in ITC buffer (20 mM HEPES pH 8.0, 150 mM NaCl, 1 mM TCEP) unless otherwise stated. Purified IKKα(10-667) EE and IKKβ(1-669) EE protein samples were dialyzed overnight against ITC buffer at 4 °C. Just before the ITC experiments, IKKα or IKKβ samples were concentrated, incubated at room temperature for 30 minutes and centrifuged at 11 000 *g* to remove eventual precipitate. The final concentrations of IKKα and IKKβ in the sample cell varied between 22 and 50 µM, depending on the measurement. HPLC purified synthetic peptides were further desalted using a Nap5 (Cytiva, #17-0853-01) column equilibrated in milliQ water, lyophilized and then resuspended in ITC buffer. Peptide concentration in the syringe varied between 220 and 975 µM, depending on the measurement.

All ITC measurements were performed using a PEAQ-ITC MALVERN instrument. The titration parameters were set as following: temperature 25 °C, reference power 10 µcal/s, feedback=high, stirring speed 750 RPM, initial delay 60 s, first injection 0.4 µL in 0.8 s and the remaining 19 injections were 2 µL in 4 s with 120 s of spacing. The data were fitted to a 1:1 binding model. Initial data processing was carried out in MicroCal PEAQ-ITC Analysis software. For thermodynamic analysis, all data were processed using NITPIC software[60] and global fitting of two datasets was carried out using SEDPHAT[61]. For some interaction pairs sample aggregation during the titration caused disturbed baselines. For this, unbiased baseline subtraction of NITPIC was instrumental in obtaining the data suitable for the analysis. The error analysis was done using error surfaces prescribed by F-statistics as implemented in SEDPHAT. The confidence intervals at 68.3% probability corresponding to one SD assuming a Gaussian error distribution were derived for K_D and ΔH best-fit values and are reported in Table 1. The binding in IKKα/pY-IκBα pep and IKKα/IRF7 pep interactions was too weak to allow for accurate thermodynamic analysis.

In vitro kinase assays

Using recombinant IKKβ. Reactions were performed in the kinase buffer (50 mM Tris-HCl at pH 8.0, 100 mM NaCl, 10 mM $MgCl_2$, 2 mM $MnCl_2$, 0.5 mg/mL BSA, 20 mM β-glycerol phosphate, 400 µM sodium orthovanadate, 2 mM DTT, and 400 µM ATP) using 0.5 nM of purified 6xHis-IKKβ(1-669) EE protein and 1 µM of purified full-length 6xHis-IκBα wt or mutant constructs.

Using endogenous IKK complex. IKK was immunoprecipitated from HEK293T cells. 3 petri dishes (100 × 15 mm) of cells at 70% confluence were induced with 10 nM recombinant TNFα (R&D Systems) for 10 minutes, and then washed twice by cold PBS. The whole-cell extracts were prepared by addition of 1 ml of lysis buffer (50 mM mM HEPES pH 8, 200 mM NaCl, 0.5% NP-40, 1 mM EDTA, 10 mM KCl, 1 mM DTT, Roche cOmplete™ protease inhibitor, 50 mM NaF, 50 mM β-glycerophosphate, and 1 mM sodium orthovanadate) and homogenized by passing through a 21-gauge needle for 5-10 times. After 30 minutes of incubation on ice, the extracts were centrifuged at 11,000 *g* and at 4 °C. The cleared supernatants were incubated with 15 µl of anti-NEMO antibody (Santa Cruz biotech) overnight at 4 °C and, then, immunoprecipitated with 150 µl of protein G Sepharose® beads (Cytiva) for 2 hours at 4 °C. The beads were washed with wash buffer (50 mM Tris, pH 8, 150 mM NaCl, 5 mM β-glycerophosphate, 0.1 mM Na orthovanadate, 10 mM $MgCl_2$, 2 mM DTT) and then resuspended with wash buffer to a final volume of 150 µl. Kinase reactions were performed in kinase buffer (defined above) using 50 µl of immunoprecipitant and 1 µM of purified full-length 6xHis-IκBα wt or mutant constructs. For evaluation of peptide inhibitory activity, the reactions were supplemented with 500 µM of synthetic IκBα pep peptide variants.

All reaction mixtures were set-up in a total volume of 150 µl and incubated at 30 °C, with 30 µl aliquots sampled at 0, 5, 10 and 30 minutes time points. Reactions were stopped by addition of Laemmli sample buffer plus heating for 5 minutes at 95 °C and analyzed on a 10% SDS-PAGE gel followed by Western blotting using anti-phospho-IκBα (Cell Signaling Technology), anti-IKKβ (Cell Signaling Technology) and anti-6xHis (Sigma) antibodies. The relative amounts of phosphorylated IκBα were quantified using ImageJ.

In cellulo inhibition of NF-κB signaling

The mRNAs coding for the mScarlet-E3-IκBα pep fusions were transcribed from the T7 promoter using HiScribe™ T7 ARCA mRNA Kit (New England Biolabs) according to the manufacturer recommendations. 0.5 µg mRNAs were electroporated in 1.10^5 MRC-5 cells using the Neon™ transfection system (Invitrogen)[62]. 24 hours after electroporation, cells were treated or not with TNFα (R&D system) at 20 ng/ml for 30 minutes. Hence, cells were fixed with 4% (w/v)

paraformaldehyde for 30 minutes and then permeabilized with 0.2% Triton X-100 for 5 minutes in PBS buffer, 10% FCS. Cells were incubated with anti-p65 antibody (1/2000 dilution) (Santa-Cruz biotechnology,) followed by an anti-mouse mAb-Alexa-Fluor 488 conjugated (Invitrogen). Coverslips were then mounted with Fluoromount G containing 4',6'–diamidino-2-phenyleindole (SouthernBiotech). Treated cells were analyzed by fluorescence microscopy (Leica DM5500B and LAS AF software). Image processing was performed using ImageJ 2.3.0. Data analysis was performed using Prism 9 software. Statistical analysis was performed by ordinary one-way ANOVA test.

Antibodies

Immunoblotting. Anti-6xHis (Sigma, H1029), anti-HA (Santa Cruz biotechnology, sc-7392), anti-IKKβ (Cell Signaling Technology, 2684), anti-IκBα (Santa Cruz biotechnology, sc-371), anti-phospho-Ser32,-Ser36-IκBα (Cell Signaling Technology, 9246), anti-Gluc (New England Biolabs, E8023, Invitrogen, PA1-181), anti-phospho-tyrosine (Millipore, 05-321), anti-HSP90 (Santa Cruz biotechnology, sc-13119).

Immunoprecipitation. Anti-NEMO (Santa Cruz biotechnology, sc-166398), anti-HA beads (Santa Cruz biotechnology, sc-7392AC), mouse IgG (Santa Cruz biotechnology, sc-2025).

Immunofluorescence. Anti-p65 (Santa Cruz biotechnology, sc-8008), Anti-mouse secondary antibody-AlexaFluor 488 (Invitrogen, A-11001).

x-ray crystallography

Crystallization. The purified IKKβ(1-669) EE construct in 20 mM HEPES pH 8, 150 mM NaCl, 2 mM TCEP was concentrated to 15 mg/ml, mixed with a 1.5 molar excess of synthetic wt IκBα pep and incubated on ice for 1 hour. Crystallization experiments were performed by the sitting drop vapor diffusion method at 277 K using a Mosquito Crystal nanolitre dispensing robot (SPT Labtech) and several commercially available screens, i.e. the Berkeley screen (prepared in-house[63]), the ProComplex suite, the Classics suite and the PEGs suite (Qiagen), the JCSG+ suite and the Wizard Classic 1 & 2 suite (Molecular Dimensions). 0.1 µl of the sample solution was mixed with 0.1 µl of the reservoir solution and equilibrated against 50 µl of reservoir solution in 96-well MRC2 sitting drop vapor diffusion crystallization plates (Molecular Dimensions). The plates were stored at 277 K and automatically imaged using a RockImager 1000 (Formulatrix).

Small initial crystals (~ 50 ×15 x 15 µm) appeared after 2 days in condition 4 of the Berkeley screen (1.8 M $(NH_4)_2SO_4$, 0.1 M Bis-Tris HCl pH 6.5, 10% 2-propanol) but appeared multiple. After manual reproduction of the condition, large single crystals (~ 500 ×80 x 40 µm) grew after 8 days. The crystals were transferred to 2 M Li_2SO_4, 0.1 M Bis-Tris HCl pH 6.5 before flash cooling in liquid nitrogen.

Data collection and processing, and structure determination. X-ray diffraction data were collected at 100 K on an EIGER X 9 M detector (Dectris) at the Proxima 2 A beamline of Synchrotron SOLEIL (Paris). 360° of data were collected using 0.1° rotation and 0.025 s exposure per image at 100% beam intensity at an energy of 12.65 keV (wavelength = 0.98 Å). The data were processed and scaled using XDS[64] before anisotropic truncation and correction was performed using the STARANISO server[65]. The crystal diffracted anisotropically to 4.2 Å (6.8 Å in the worst direction) and belonged to the C-centered monoclinic space group C2 with unit cell dimensions a = 226.3 Å, b = 136.8 Å, c = 204.4 Å, β = 91.45°.

The structure was solved by molecular replacement using PHASER[66] in the PHENIX suite[67] using a monomer extracted from the structure of the asymmetric dimer of human IκB kinase β[14] (PDB ID 4KIK) as a search model. The asymmetric unit contains five copies of the protein (two dimers, and one monomer that forms a dimer with itself over a crystallographic 2-fold rotation axis), with a corresponding Matthews' coefficient of 4.1 $Å^3$ Da^{-1} and a solvent content of 69.9 %. Refinement of the structures was performed using PHENIX[68] and BUSTER[69] followed by with iterative model building in COOT[70]. Data collection and refinement statistics are summarized in Supplementary Table 1.

Cross-linking mass spectrometry (CLMS)

Sample preparation. Purified 6xHis-IKKβ(1-699) EE protein in 20 mM HEPES, pH 8.0, 150 mM NaCl, 5% glycerol and 1 mM TCEP was adjusted to a concentration of 12 µM and incubated with a 10-fold molar excess of C308L/R314K IκBα pep on ice for 2 hours in the presence of 10 mM $MgCl_2$. For crosslinking with EDC/Sulfo-NHS, the IKKβ/peptide mixture was incubated with 5 mM EDC (Thermo Fisher Scientific) and 10 mM Sulfo-NHS (Thermo Fisher Scientific) at RT for 30 minutes in activation buffer (100 mM MES, pH 5,5, 500 mM NaCl, 10 mM $MgCl_2$, 2.5% glycerol and 1 mM TCEP) in a total volume of 100 µL. Then, an equal volume of 10 × PBS was added to increase the pH of the sample, which was further incubated at RT for 2 hours. To quench the crosslinking reaction hydroxylamine (Thermo Fisher Scientific) was added to a final concentration of 10 mM. For cross-linking with BS3, the IKKβ/peptide mixture was incubated with 600 µM BS3 at 4 °C for 2 hours in a total volume of 100 µL, then the reaction was quenched by incubation with 50 mM fresh ammonium bicarbonate at RT for 30 minutes. For crosslinking with Sulfo-SDA, the IKKβ/peptide mixture was incubated with different concentrations (0.2, 0.5, 1, and 2 mM) of Sulfo-SDA (Thermo Fisher Scientific) at 4 °C for 2 hours in the dark. Then, the mixture was photoactivated by UV irradiation for 15 or 30 minutes. The UV lamp (set at 6 watts, 365 nm) was placed at 2 cm from the sample. Finally, the reaction was quenched by incubation with 50 mM fresh ammonium bicarbonate at RT for 30 minutes.

Crosslinked samples were separated using an 8% SDS-PAGE that was stained using Quick Coomassie (Neo Biotech). IKKβ-peptide bands were cut into about 1 mm × 1 mm cubes, dried by acetonitrile, and stored at −20 °C until analysis.

Proteins in the gel bands were reduced and cysteines were modified with iodoacetamide. Digestion with trypsin (Thermo Scientific Pierce) was occurred overnight at 37 °C. The resulting tryptic peptides were extracted and desalted using C18 StageTips. Samples were eluted just prior to analysis by LC-MS/MS.

LC-MS analysis. LC-MS/MS analysis was performed on an Orbitrap Fusion Lumos Tribrid mass spectrometer (Thermo Fisher) coupled online with an Ultimate 3000 RSLCnano system (Dionex, Thermo Fisher). MS data were acquired on one biological sample per condition. Samples were separated on a 50-cm EASY-Spray column (Thermo Fisher). Mobile phase A consisted of 0.1 % (v/v) formic acid and mobile phase B of 80 % (v/v) acetonitrile with 0.1 % (v/v) formic acid. Flow rates were 0.3 µl/minute using a gradient from 2 % to 45 % mobile phase B over 90 minutes. Mass spec data were acquired in data-dependent mode using the top-speed setting with a three second cycle time. For every cycle, the full scan mass spectrum was recorded using the Orbitrap at a resolution of 120,000 in the range of 400 to 1600 m/z. Ions with a precursor charge state between 3+ and 7+ were isolated and fragmented. Each precursor was fragmentated by higher-energy Collisional Dissociation (HCD) at 26%, 28%, and 30%. The fragmentation spectra were then recorded in the Orbitrap with a resolution of 60,000. Dynamic exclusion was enabled with single repeat count and 60-seconds exclusion duration.

Data analysis. A recalibration of the precursor m/z was conducted based on high-confidence (<1 % False Discovery Rate, FDR) linear peptide identifications. The re-calibrated peak lists were searched against the sequences and the reversed sequences (as decoys) of crosslinked peptides using the Xi software suite (v.1.7.6.4) for identification[71]. The following parameters were used

for each crosslinker: up to 3 missed cleavages; up to two missing monoisotopic peaks; 2 ppm MS1 tolerance; 5 ppm MS2 tolerance. Variable modifications were: deamidation on Asparagine; methylation on Glutamic acid; N-terminal Glutamate to Pyroglutamate.

It is not possible to do an accurate false discovery rate threshold with such small datasets, so instead we filtered to matches with > 30% sequence coverage on each peptide and a delta score that was > 30% of the score, for all crosslinkers. Additionally, for SDA, there had to be at least one crosslinker containing fragment for each peptide. This filtering was done with xiFDR v.2.2.beta5[71]. No decoys passed these thresholds for any of the datasets.

Protein-peptide docking calculations

The IKKβ/IκBα pep complex model was calculated using the HADDOCK2.4 webserver[34,72]. The IKKβ AB homodimer (Supplementary Fig. 4) was used as a starting structure. For the structure calculations IκBα pep was generated in an extended conformation. The IκBα pep was docked to one face of the symmetric IKKβ homodimer. IKKβ interface residues binding to IκBα pep were first identified from the quantitative analysis of CLMS data using the DisVis[34] tool in "quick scanning" mode with an extended conformation of IκBα pep (Supplementary Fig. 6a). These residues and the whole peptide were maintained as active throughout the docking protocol (Supplementary Data 4). Over 30 unique distance restrains derived from CLMS data were imposed as unambiguous restraints using an OR statement, so that they could map to residues from either chain of the IKKβ homodimer (Supplementary Data 5). Restraints derived from links obtained with sulfo-SDA spanned 2.5 - 22.5 Å (Cb-Cb), whereas EDC/NHS crosslinks were set to 1.5-7 Å (Cb - Cb). The number of molecular dynamics steps in the rigid body and flexible refinement stages was increased to allow for sampling of larger conformational changes. In particular, the steps for rigid body high temperature torsion angle dynamics, first rigid body cooling, second cooling stage and fully flexible interface third cooling stage were all increased to 2000. 1000 structures were generated in it0 and the top 200 structures were selected for refinement and clustered. The entire peptide was set to be fully flexible. Docking solutions were clustered on the basis of interface r.m.s.d. with a cutoff of 5 Å. The best scoring structure from the best scoring cluster is taken as solution.

Molecular graphics. All molecular images were made using the PyMOL software[73] unless otherwise stated.

Reporting summary

Further information on research design is available in the Nature Portfolio Reporting Summary linked to this article.

Data availability

Coordinates of the refined x-ray structure of IKKβ and structure factor amplitudes generated in this study have been deposited in the PDB database under accession number 8OMV. CLMS raw and processed data are available on JPOST and ProteomeXchange database with identifier PXD037534. All other data generated in this study are provided in the main text, Supplementary Information and Data files, and in the Source Data files. Source data are provided with this paper.

References

1. Taniguchi, K. & Karin, M. NF-κB, inflammation, immunity and cancer: coming of age. *Nat. Rev. Immunol.* **18**, 309–324 (2018).
2. Hinz, M. & Scheidereit, C. The IκB kinase complex in NF-κB regulation and beyond. *Embo Rep.* **15**, 46–61 (2014).
3. Rothwarf, D. M., Zandi, E., Natoli, G. & Karin, M. IKK-γ is an essential regulatory subunit of the IκB kinase complex. *Nature* **395**, 297–300 (1998).
4. Zandi, E., Rothwarf, D. M., Delhase, M., Hayakawa, M. & Karin, M. The IκB kinase complex (IKK) Contains two kinase subunits, IKKα and IKKβ, necessary for IκB phosphorylation and NF-κB activation. *Cell* **91**, 243–252 (1997).
5. Yamaoka, S. et al. Complementation cloning of NEMO, a component of the IκB kinase complex essential for NF-κB activation. *Cell* **93**, 1231–1240 (1998).
6. Israël, A. The IKK complex, a central regulator of NF-κB activation. *Csh Perspect. Biol.* **2**, a000158 (2010).
7. Karin, M. & Ben-Neriah, Y. Phosphorylation meets ubiquitination: the control of NF-κB activity. *Annu Rev. Immunol.* **18**, 621–663 (2000).
8. Yaron, A. et al. Inhibition of NF-κB cellular function via specific targeting of the IκB-ubiquitin ligase. *Embo J.* **16**, 6486–6494 (1997).
9. Senftleben, U. et al. Activation by IKKα of a second, evolutionary conserved, NF-κB signaling pathway. *Science* **293**, 1495–1499 (2001).
10. Xiao, G., Fong, A. & Sun, S.-C. Induction of p100 processing by NF-κB-inducing kinase involves docking IκB kinase α (IKKα) to p100 and IKKα-mediated phosphorylation*. *J. Biol. Chem.* **279**, 30099–30105 (2004).
11. Xu, G. et al. Crystal structure of inhibitor of κB kinase β. *Nature* **472**, 325–330 (2011).
12. Polley, S. et al. A structural basis for IκB kinase 2 activation via oligomerization-dependent trans auto-phosphorylation. *Plos Biol.* **11**, e1001581 (2013).
13. Polley, S. et al. Structural basis for the activation of IKK1/α. *Cell Rep.* **17**, 1907–1914 (2016).
14. Liu, S. et al. Crystal structure of a human IκB kinase β asymmetric dimer. *J. Biol. Chem.* **288**, 22758–22767 (2013).
15. Schröfelbauer, B., Polley, S., Behar, M., Ghosh, G. & Hoffmann, A. NEMO ensures signaling specificity of the pleiotropic IKKβ by directing its kinase activity toward IκBα. *Mol. Cell* **47**, 111–121 (2012).
16. Maubach, G., Schmädicke, A.-C. & Naumann, M. NEMO links nuclear factor-κB to human diseases. *Trends Mol. Med* **23**, 1138–1155 (2017).
17. Catici, D. A. M., Horne, J. E., Cooper, G. E. & Pudney, C. R. Polyubiquitin drives the molecular interactions of the NF-κB essential modulator (NEMO) by allosteric regulation. *J. Biol. Chem.* **290**, 14130–14139 (2015).
18. Rahighi, S. et al. Specific recognition of linear ubiquitin chains by NEMO is important for NF-κB activation. *Cell* **136**, 1098–1109 (2009).
19. Tokunaga, F. et al. Involvement of linear polyubiquitylation of NEMO in NF-κB activation. *Nat. Cell Biol.* **11**, 123–132 (2009).
20. Laplantine, E. et al. NEMO specifically recognizes K63-linked polyubiquitin chains through a new bipartite ubiquitin-binding domain. *Embo J.* **28**, 2885–2895 (2009).
21. Scholefield, J. et al. Super-resolution microscopy reveals a preformed NEMO lattice structure that is collapsed in incontinentia pigmenti. *Nat. Commun.* **7**, 12629 (2016).
22. Du, M., Ea, C.-K., Fang, Y. & Chen, Z. J. Liquid phase separation of NEMO induced by polyubiquitin chains activates NF-κB. *Mol. Cell* **82**, 2415–2426.e5 (2022).
23. Antonia, R. J., Hagan, R. S. & Baldwin, A. S. Expanding the view of IKK: new substrates and new biology. *Trends Cell Biol.* **31**, 166–178 (2021).
24. Hoshino, K. et al. IκB kinase-α is critical for interferon-α production induced by Toll-like receptors 7 and 9. *Nature* **440**, 949–953 (2006).
25. Chariot, A. The NF-κB-independent functions of IKK subunits in immunity and cancer. *Trends Cell Biol.* **19**, 404–413 (2009).
26. Anest, V. et al. A nucleosomal function for IκB kinase-α in NF-κB-dependent gene expression. *Nature* **423**, 659–663 (2003).
27. Yamamoto, Y., Verma, U. N., Prajapati, S., Kwak, Y.-T. & Gaynor, R. B. Histone H3 phosphorylation by IKKα is critical for cytokine-induced gene expression. *Nature* **423**, 655–659 (2003).

28. Miller, C. J. & Turk, B. E. Homing in: mechanisms of substrate targeting by protein kinases. *Trends Biochem Sci.* **43**, 380–394 (2018).
29. Zandi, E., Chen, Y. & Karin, M. Direct phosphorylation of IκB by IKKα and IKKβ: discrimination between free and NF-κB-bound substrate. *Science* **281**, 1360–1363 (1998).
30. Kawai, H., Nie, L. & Yuan, Z.-M. Inactivation of NF-κB-dependent cell survival, a novel mechanism for the proapoptotic function of c-Abl. *Mol. Cell. Biol.* **22**, 6079–6088 (2002).
31. Vigneron, M. et al. Self-associating peptides for modular bifunctional conjugation of tetramer macromolecules in living cells. *Bioconjugate Chem.* **30**, 1734–1744 (2019).
32. O'Reilly, F. J. & Rappsilber, J. Cross-linking mass spectrometry: methods and applications in structural, molecular and systems biology. *Nat. Struct. Mol. Biol.* **25**, 1000–1008 (2018).
33. Belsom, A., Schneider, M., Fischer, L., Brock, O. & Rappsilber, J. Serum albumin domain structures in human blood serum by mass spectrometry and computational biology. *Mol. Cell Proteom.* **15**, 1105–1116 (2016).
34. van Zundert, G. C. P. et al. The haddock2.2 web server: user-friendly integrative modeling of biomolecular complexes. *J. Mol. Biol.* **428**, 720–725 (2016).
35. Krystkowiak, I. & Davey, N. E. SLiMSearch: a framework for proteome-wide discovery and annotation of functional modules in intrinsically disordered regions. *Nucleic Acids Res* **45**, gkx238 (2017).
36. Caillaud, A., Hovanessian, A. G., Levy, D. E. & Marié, I. J. Regulatory serine residues mediate phosphorylation-dependent and phosphorylation-independent activation of interferon regulatory factor 7*. *J. Biol. Chem.* **280**, 17671–17677 (2005).
37. tenOever, B. R. et al. Activation of TBK1 and IKKε kinases by vesicular stomatitis virus infection and the role of viral ribonucleoprotein in the development of interferon antiviral immunity. *J. Virol.* **78**, 10636–10649 (2004).
38. Chen, W. et al. Insights into interferon regulatory factor activation from the crystal structure of dimeric IRF5. *Nat. Struct. Mol. Biol.* **15**, 1213–1220 (2008).
39. Yokoyama, K. et al. BANK regulates BCR-induced calcium mobilization by promoting tyrosine phosphorylation of IP3 receptor. *EMBO J.* **21**, 83–92 (2002).
40. Georg, I., Díaz-Barreiro, A., Morell, M., Pey, A. L. & Alarcón-Riquelme, M. E. BANK1 interacts with TRAF6 and MyD88 in innate immune signaling in B cells. *Cell. Mol. Immunol.* **17**, 954–965 (2020).
41. Ma, X. et al. Molecular basis of Tank-binding kinase 1 activation by transautophosphorylation. *Proc. Natl Acad. Sci.* **109**, 9378–9383 (2012).
42. Newlon, M. G. et al. A novel mechanism of PKA anchoring revealed by solution structures of anchoring complexes. *Embo J.* **20**, 1651–1662 (2001).
43. Sarma, G. N. et al. Structure of D-AKAP2:PKA RI complex: insights into AKAP specificity and selectivity. *Structure* **18**, 155–166 (2010).
44. Burke, J. R., Miller, K. R., Wood, M. K. & Meyers, C. A. The multisubunit IκB kinase complex shows random sequential kinetics and is activated by the c-terminal domain of IκBα*. *J. Biol. Chem.* **273**, 12041–12046 (1998).
45. Burke, J. R., Wood, M. K., Ryseck, R.-P., Walther, S. & Meyers, C. A. Peptides corresponding to the N and C termini of IκB-α, -β, and -ε as probes of the two catalytic subunits of IκB kinase, IKK-1 and IKK-2*. *J. Biol. Chem.* **274**, 36146–36152 (1999).
46. Huynh, Q. K. et al. Characterization of the recombinant IKK1/IKK2 heterodimer mechanisms regulating kinase activity. *J. Biol. Chem.* **275**, 25883–25891 (2000).
47. Schröfelbauer, B. & Hoffmann, A. How do pleiotropic kinase hubs mediate specific signaling by TNFR superfamily members? *Immunol. Rev.* **244**, 29–43 (2011).
48. Liberatore, R. A., Goff, S. P. & Nunes, I. NF-κB activity is constitutively elevated in c-Abl null fibroblasts. *Proc. Natl Acad. Sci.* **106**, 17823–17828 (2009).
49. Garai, Á. et al. Specificity of linear motifs that bind to a common mitogen-activated protein kinase docking groove. *Sci. Signal* **5**, ra74 (2012).
50. Bollen, M., Peti, W., Ragusa, M. J. & Beullens, M. The extended PP1 toolkit: designed to create specificity. *Trends Biochem Sci.* **35**, 450–458 (2010).
51. Prescott, J. A. & Cook, S. J. Targeting IKKβ in cancer: challenges and opportunities for the therapeutic utilisation of IKKβ inhibitors. *Cells* **7**, 115 (2018).
52. May, M. J. et al. Selective inhibition of NF-κB activation by a peptide that blocks the interaction of NEMO with the IκB kinase complex. *Science* **289**, 1550–1554 (2000).
53. Agou, F. et al. Inhibition of NF-κB activation by peptides targeting NF-κB essential modulator (NEMO) oligomerization. *J. Biol. Chem.* **279**, 54248–54257 (2004).
54. Ko, M. S. et al. Regulatory subunit NEMO promotes polyubiquitin-dependent induction of NF-κB through a targetable second interaction with upstream activator IKK2. *J. Biol. Chem.* **298**, 101864 (2022).
55. Cassonnet, P. et al. Benchmarking a luciferase complementation assay for detecting protein complexes. *Nat. Methods* **8**, 990–992 (2011).
56. Morgenstern, J. P. & Land, H. A series of mammalian expression vectors and characterisation of their expression of a reporter gene in stably and transiently transfected cells. *Nucleic Acids Res* **18**, 1068–1068 (1990).
57. Kolesnikova, O. et al. HR-Bac, a toolbox based on homologous recombination for expression, screening and production of multiprotein complexes using the baculovirus expression system. *Sci. Rep.-uk* **12**, 2030 (2022).
58. Behrendt, R., White, P. & Offer, J. Advances in Fmoc solid-phase peptide synthesis. *J. Pept. Sci.* **22**, 4–27 (2016).
59. Schnölzer, M., Alewood, P., Jones, A., Alewood, D. & Kent, S. B. H. In situ neutralization in boc-chemistry solid phase peptide synthesis. *Int J. Pept. Res Ther.* **13**, 31–44 (2007).
60. Scheuermann, T. H. & Brautigam, C. A. High-precision, automated integration of multiple isothermal titration calorimetric thermograms: New features of NITPIC. *Methods* **76**, 87–98 (2015).
61. Brautigam, C. A., Zhao, H., Vargas, C., Keller, S. & Schuck, P. Integration and global analysis of isothermal titration calorimetry data for studying macromolecular interactions. *Nat. Protoc.* **11**, 882–894 (2016).
62. Juncker, T., Chatton, B. & Donzeau, M. The prodigious potential of mRNA electrotransfer as a substitute to conventional DNA-based transient transfection. *Cells* **12**, 1591 (2023).
63. Pereira, J. H., McAndrew, R. P., Tomaleri, G. P. & Adams, P. D. Berkeley screen: a set of 96 solutions for general macromolecular crystallization. *J. Appl Crystallogr* **50**, 1352–1358 (2017).
64. Kabsch, W. XDS. *Acta Crystallogr Sect. D. Biol. Crystallogr* **66**, 125–132 (2010).
65. Tickle, I. et al. *STARANISO* Cambridge, United Kingdom: Global Phasing Ltd. (2019).
66. McCoy, A. J. Solving structures of protein complexes by molecular replacement with Phaser. *Acta Crystallogr Sect. D. Biol. Crystallogr* **63**, 32–41 (2007).
67. Liebschner, D. et al. Macromolecular structure determination using X-rays, neutrons and electrons: recent developments in Phenix. *Acta Crystallogr Sect. D.* **75**, 861–877 (2019).
68. Afonine, P. V. et al. Towards automated crystallographic structure refinement with phenix.refine. *Acta Crystallogr Sect. D.* **68**, 352–367 (2012).

69. Bricogne, G. et al. *BUSTER Version 2.10.4*. Cambridge, United Kingdom: Global Phasing Ltd. (2021).
70. Emsley, P., Lohkamp, B., Scott, W. G. & Cowtan, K. Features and development of Coot. *Acta Crystallogr Sect. D. Biol. Crystallogr* **66**, 486–501 (2010).
71. Mendes, M. L. et al. An integrated workflow for crosslinking mass spectrometry. *Mol. Syst. Biol.* **15**, e8994 (2019).
72. Honorato, R. V. et al. Structural biology in the clouds: The WeNMR-EOSC ecosystem. *Front. Mol. Biosci.* **8**, 729513 (2021).
73. Schrödinger, L. & DeLano, W. *PyMOL*. (2020).
74. Pettersen, E. F. et al. UCSF Chimera—a visualization system for exploratory research and analysis. *J. Comput. Chem.* **25**, 1605–1612 (2004).

Acknowledgements

The authors are grateful to Alexander Hoffmann (UCLA, USA), Fabrice Agou (Institut Pasteur, France), Jean Cavarelli, Partick Schultz and Philippe Dumas (IGBMC, France), and Massimo Tommasino (IRRCS of Bari, Italy) for insightful discussions. The authors also thank Gunter Stier (University of Heidelberg, Germany) for providing material; Marie-Laure Straub (CNRS-UMR7242, France) for technical assistance; Denise Martinez-Zapien, Renaud Wagner (CNRS-UMR7242, France), and Laurent Bianchetti and Pascal Eberling (IGBMC, France) for help at the initial stages of the project. The MBioFaSt (IBMC, France) and Structural Biology (IGBMC-CBI, France) platforms funded by Instruct-ERIC are acknowledged for technological support. This work received institutional support from CNRS and the University of Strasbourg. The work was supported by grants from Agence Nationale de la Recherche (ANR JCJC, ref. ANR-13-JSV8-0004-01), 'Ligue contre le Cancer' (CCIRGE), 'Fondation pour La Recherche Medicale' (Equipes FRM, ref. DEQ20180339231), ITI Innovec (IdEx ANR-10-IDEX-0002), STRAT'US(ANR-20-SFRI-0012)) and 'Alsace contre le Cancer' and Instruct-ERIC (PID 11382) to KZ. Additional funding sources include ITI IMCBio+ (IdEx ANR-10-IDEX-0002, SFRI-STRAT'US ANR-20-SFRI-0012 and EUR IMCBio, ANR-17-EURE-0023) and FRISBI (ANR-10-INBS-0005) to IGBMC-CBI.

Author contributions

A.C. and K.Z. designed this study. C.L., S.M., D.D., and M.F. prepared recombinant protein samples, performed in vitro and *in cellulo* binding, and in vitro kinase activity experiments. T.B, V.T., and K.B.: performed peptide synthesis and/or ITC experiments. N.B. and S.P. performed insect cell protein expression. K.S. and M.D. performed *in cellulo* functional experiments. C.L., S.M., and P.P.C. conducted crystallization experiments. A.M.E. solved the x-ray structure. C.L. and FOR performed CLMS experiments. A.G. performed docking calculations. N.D. performed bioinformatics analyzes. G.O., A.P., J.R., A.C., and K.Z. provided supervision. K.Z. wrote the manuscript with the help of all co-authors.

Competing interests

An application for a patent on the YDDΦxΦ sequences identified in this study and their uses has been deposited. Applicants: Centre National de la Recherche Scientifique, Université de Strasbourg, Université de Liège; inventors: K. Zanier, C. Li, K. Shostak, M. Donzeau, A. Chariot; application number: TCT/EP2024/065645; status of application: filed not published. The remaining authors declare no competing interests.

Additional information

Supplementary information The online version contains supplementary material available at https://doi.org/10.1038/s41467-024-52076-0.

Correspondence and requests for materials should be addressed to Katia Zanier.

Peer review information *Nature Communications* thanks Attila Remenyi, Guozhou Xu and the other, anonymous, reviewer(s) for their contribution to the peer review of this work. A peer review file is available.